Biosynthesis of the Metalloclusters of Nitrogenases

Yilin Hu[1] and Markus W. Ribbe[1,2]

[1]Department of Molecular Biology and Biochemistry and [2]Department of Chemistry, University of California, Irvine, California 92697-2025; email: yilinh@uci.edu, mribbe@uci.edu

Annu. Rev. Biochem. 2016. 85:455–83

First published online as a Review in Advance on February 1, 2016

The *Annual Review of Biochemistry* is online at biochem.annualreviews.org

This article's doi: 10.1146/annurev-biochem-060614-034108

Keywords

assembly, M-cluster, V-cluster, P-cluster, [Fe_4S_4], radical SAM

Abstract

Nitrogenase is a versatile metalloenzyme that is capable of catalyzing two important reactions under ambient conditions: the reduction of nitrogen (N_2) to ammonia (NH_3), a key step in the global nitrogen cycle; and the reduction of carbon monoxide (CO) and carbon dioxide (CO_2) to hydrocarbons, two reactions useful for recycling carbon waste into carbon fuel. The molybdenum (Mo)- and vanadium (V)-nitrogenases are two homologous members of this enzyme family. Each of them contains a P-cluster and a cofactor, two high-nuclearity metalloclusters that have crucial roles in catalysis. This review summarizes the progress that has been made in elucidating the biosynthetic mechanisms of the P-cluster and cofactor species of nitrogenase, focusing on what is known about the assembly mechanisms of the two metalloclusters in Mo-nitrogenase and giving a brief account of the possible assembly schemes of their counterparts in V-nitrogenase, which are derived from the homology between the two nitrogenases.

Contents

INTRODUCTION

Nitrogenase is a versatile metalloenzyme that is capable of reducing various substrates under ambient conditions (1–6). Best known for its function in biological nitrogen fixation, nitrogenase catalyzes the reduction of nitrogen (N_2) to ammonia (NH_3), a key step in the global nitrogen cycle (1). Recently, nitrogenase has been shown to reduce carbon monoxide (CO) and carbon dioxide (CO_2) to hydrocarbons, two reactions that are important for recycling carbon waste into useful fuel products (7–14). Interestingly, the nitrogenase-catalyzed reactions of N_2 and CO reduction mirror two important industrial processes: the Haber–Bosch process, which combines N_2 and hydrogen (H_2) into NH_3 (15), and the Fischer–Tropsch process, which combines CO and H_2 into carbon fuels (16). However, contrary to the industrial processes, the nitrogenase-catalyzed reactions use protons (H^+) instead of the expensive synthesis gas, H_2, and they occur under ambient conditions, making this enzyme a potential template for the future development of cost-efficient strategies for producing ammonia and hydrocarbons.

The best studied nitrogenase is the molybdenum (Mo) nitrogenase from *Azotobacter vinelandii* (1, 2, 4, 5), which consists of two component proteins. One, designated the iron (Fe) protein (NifH), is a homodimer containing a subunit-bridging ($[Fe_4S_4]$) cluster and an adenosine triphosphate (ATP)-binding site within each subunit; the other, designated the molybdenum–iron protein (NifDK), is an $\alpha_2\beta_2$-tetramer containing a P-cluster ($[Fe_8S_7]$) at each α/β-subunit interface and an M-cluster ($[MoFe_7S_9C$-homocitrate$]$) within each α-subunit (17–20). Upon substrate turnover, the two components form a functional complex (21, 22), permitting electrons to be transferred concomitantly with ATP hydrolysis from the $[Fe_4S_4]$ cluster of NifH via the P-cluster to the M-cluster of NifDK, where substrate reduction occurs upon accumulation of a sufficient amount of electrons (**Figure 1*a*,*b***). The arrangement of the components of the electron-transfer pathway highlights the key roles of metalloclusters in nitrogenase catalysis.

Biologically important and chemically unprecedented, the M- and P-clusters have attracted considerable attention since their discovery. The M-cluster (also called FeMoco or FeMo cofactor) is buried within the α-subunit of NifDK, 10 Å beneath the protein surface (17–20). Apart from the complexity of its metal–sulfur (S) core, the M-cluster is also noted for the presence of an organic homocitrate moiety and a μ_6-interstitial carbide in its structure (**Figure 1*d***). The homocitrate entity, which is -4 when its hydroxyl group is deprotonated, is believed to give the M-cluster an overall negative charge despite a proposed charge of $+1$ or $+3$ for the metal–sulfur core of this cluster in the resting state (23–27). The interstitial carbide, which cannot be exchanged upon substrate turnover, likely serves as an anchor that stabilizes the structure of the M-cluster (28,

29), although a function of this atom in indirectly modulating the reactivity of the M-cluster or directly interacting with the substrate cannot be ruled out (30). The P-cluster is bridged at the α/β-subunit interface of NifDK, 14 Å away from the M-cluster (17–19). In the presence of excess dithionite, the P-cluster assumes an all-ferrous diamagnetic state (designated the P^N state). Upon oxidation by indigo disulfonate (IDS), however, the P-cluster is converted to a stable $S =$ integer (3 or 4) state (designated the P^{OX} state), which can be recognized by a characteristic $g = 11.8$ signal in parallel-mode electron paramagnetic resonance (EPR) analysis (31–33). The redox conversion between the P^N and P^{OX} state is accompanied by a change in the core structure of the P-cluster (**Figure 1*e***), as well as by a modification in the ligation pattern (34, 35).

The vanadium (V) nitrogenase is an alternative nitrogenase that shares a significant degree of homology with its Mo counterpart in protein sequence and cluster composition (3, 6, 36, 37). Like Mo-nitrogenase, the V-nitrogenase (38–42) consists of two component proteins: a homodimeric iron protein (VnfH) that contains a subunit-bridging $[Fe_4S_4]$ cluster and an ATP-binding site per subunit, and an $\alpha_2\beta_2\delta_4$-octameric vanadium–iron protein (VnfDGK) that contains a P^V-cluster (an $[Fe_4S_4]$-like cluster pair) at each α/β-subunit interface and a V-cluster ($[VFe_7S_9C$-homocitrate]) within each α-subunit (**Figure 1*c*,*f*,*g***). Catalysis by V-nitrogenase is believed to follow the same mode of action as that by Mo-nitrogenase, forming a complex between VnfH and VnfDGK that enables the interprotein ATP-dependent electron transfer from the $[Fe_4S_4]$ cluster of VnfH via the P^V-cluster to the V-cluster, where substrate reduction takes place (**Figure 1*c***). The V-cluster (also called FeVco or FeV cofactor) is highly homologous to the M-cluster in composition and structure, except for the substitution of V for Mo at one end of the cluster (41, 42). Likewise, the P^V-cluster is similar to the P-cluster, although the P^V-cluster assumes a more open conformation in which the two subcluster modules are more separated from each other (41, 43). The homologous, yet distinct, features of the metalloclusters in V- and Mo-nitrogenases underline the similar, yet distinct, activity profiles of these two nitrogenases, particularly an approximately 800-fold higher activity of the V-nitrogenase in CO reduction relative to that of its Mo counterpart (8).

Interestingly, the same similar, yet distinct, theme is also illustrated by the biosynthetic strategies of these closely related metalloclusters, defining nature's approach to diversified functions through variations of a common core of catalytic centers. This article provides an overview of the biosynthesis of the complex metalloclusters of nitrogenases, focusing on what is known about the assembly mechanisms of the M- and P-clusters and giving a brief account of the possible assembly schemes of the V- and P^V-clusters based on the homology between Mo- and V-nitrogenases.

BIOSYNTHESIS OF THE COFACTOR

The M-cluster of the Mo-nitrogenase consists of $[Fe_4S_3]$ and $[MoFe_3S_3]$ subclusters, bridged by three μ_2-belt sulfur atoms and one μ_6-interstitial carbide atom (**Figure 1*d***); additionally, it has an organic homocitrate moiety attached to its Mo end through 2-hydroxy and 2-carboxyl groups (17–20). Despite its structural complexity, the M-cluster is ligated by only two ligands in the α-subunit of NifDK: $Cys^{\alpha 275}$, which coordinates the Fe end of the cluster, and $His^{\alpha 442}$, which coordinates the opposite Mo end of the cluster. Compared with the M-cluster, the V-cluster of V-nitrogenase has a nearly identical metal–sulfur core, except for the substitution of V for Mo (**Figure 1*f***); further, the Cys and His ligands are conserved in the primary sequence of the α-subunit of VnfDGK (see Delivery of the Cofactor to Its Target Binding Site), suggesting that the V-cluster is coordinated by these two ligands in the same manner as that observed in the case of the M-cluster (38, 39, 41, 42). Such coordination enables an ex situ assembly scheme for both cofactors (**Figure 2**), allowing them to be synthesized elsewhere before they are inserted into their respective binding sites in the α-subunits of NifDK and VnfDGK. The results of previous studies

have led to the proposal that a number of *nif* and *vnf* gene products are required for the assembly of these cofactors (44–79). Biochemical, spectroscopic, and structural studies have narrowed this list down to a minimum set of gene products that are crucial for a three-stage assembly scheme of the cofactor (4, 44, 80–85), starting from the formation of an 8Fe core of the cofactor, continuing with the maturation of the 8Fe core into a cofactor, and completing upon delivery of the cofactor to its target binding site (**Figure 2**).

Formation of the 8Fe Core of the Cofactor

The assembly of the core structure of the cofactor is launched by NifS and NifU, which mobilize Fe and S for the formation of small FeS building blocks. NifS is a pyridoxal phosphate-dependent cysteine desulfurase, which presumably forms a protein-bound cysteine persulfide that is donated to NifU for the sequential formation of $[Fe_2S_2]$ and $[Fe_4S_4]$ clusters (45–51). A pair of $[Fe_4S_4]$ clusters are then delivered from NifU to NifB and processed into an 8Fe core of the cofactor on NifB (**Figure 2**). The biosynthetic pathways of the M- and V-clusters are believed to be identical until this point, both using NifS, NifU, and NifB to generate a common core structure for further processing.

The indispensable role of NifB in cofactor assembly was suggested by the observation of a loss of nitrogenase activity in the crude extracts of *nifB*-deletion strains (52–55) and was confirmed by the characterization of a cofactor-deficient form of NifDK (designated apo-NifDK or Δ*nifB*-NifDK) from a *nifB*-deletion strain of *A. vinelandii* (52, 86). Sequence analysis has revealed the presence of a number of conserved ligands in NifB that could accommodate the coordination of the entire complement of the Fe atoms of the cofactor; moreover, it has identified NifB as a radical *S*-adenosyl-L-methionine (SAM)-dependent enzyme containing a CxxxCxxC motif for the ligation of a SAM-binding $[Fe_4S_4]$ cluster (84). Consistent with the sequence-based predictions, two clusters were identified on NifB: One, designated the K-cluster, consists of a pair of $[Fe_4S_4]$ clusters that can be used as the building blocks for the 8Fe core (**Figure 3*a***); the other, designated the SAM-cluster, is an $[Fe_4S_4]$ cluster that is associated with the SAM-binding motif (87). Together, the K- and SAM-clusters give rise to a composite $S = 1/2$ EPR signal at $g = 2.02$, 1.95, and 1.90 (**Figure 4*a***). Interestingly, this composite signal disappears upon the addition of SAM

Figure 1

Structures of Mo- and V-nitrogenases and their associated metal centers. (*a*,*b*) $MgADP{\bullet}AlF_4^-$-stabilized NifH–NifDK complex (*a*, ribbon presentation; *b*, schematic presentation) and (*c*) $MgADP{\bullet}AlF_4^-$-stabilized VnfH–VnfDGK complex. The $MgADP{\bullet}AlF_4^-$, $[Fe_4S_4]$ cluster, P/P^V-cluster, and M/V-cluster are shown as space-filling models. The structure of the Mo-nitrogenase was rendered based on X-ray crystallographic data (Protein Data Bank identification number: 1N2C), whereas the hypothetical structure of the V-nitrogenase was rendered based on a combination of biochemical and spectroscopic data (3, 6). The two subunits of NifH and VnfH are colored, respectively, in shades of gray and yellow; the D (α)- and K (β)-subunits of NifDK and VnfDGK are colored, respectively, in shades of orange and blue. The G (δ)-subunit of VnfDGK is shown in white. Crystal structures of the (*d*) M-cluster and (*e*, *top*) P^N and (*e*, *bottom*) P^{OX} states of the P-cluster. The clusters are shown as ball-and-stick models. PYMOL (**https://www.pymol.org/**) was used to generate these structural models (Protein Data Bank identification numbers: 3U7Q, 1M1N, and 3MIN). X-ray absorption spectroscopy and extended X-ray absorption fine structure–derived structures of the (*f*) V-cluster and (*g*) P^V-cluster. The clusters are shown as ball-and-stick models. PYMOL was used to generate these structural models (6). Atoms are colored as follows: iron, orange; sulfur, yellow; molybdenum, cyan; oxygen, red; carbon, gray; nitrogen, blue; magnesium, green; aluminum, azure; fluorine, light blue; vanadium, dark gray. Abbreviations: ADP, adenosine diphosphate; AlF_4^-, aluminum tetrafluoride; Fe, iron; HC, homocitrate; Mg, magnesium; Mo, molybdenum; S, sulfur; V, vanadium.

(87), which implies that the K- and SAM-clusters are likely to be located in close proximity to each other and that the response of the SAM-cluster to SAM is coupled to the conversion of the K-cluster to another cluster species. Indeed, the disappearance of the $S = 1/2$ signal is accompanied by the appearance of a $g = 1.94$ signal (**Figure 4*b***) (87), which originates from an $[Fe_8S_9C]$ cluster (designated the L-cluster) that closely resembles the core structure of a mature cofactor, except for the homocitrate-free all-iron composition (88–91). This observation is exciting, as it points to a novel synthetic route employed by NifB that couples and rearranges two $[Fe_4S_4]$ clusters into

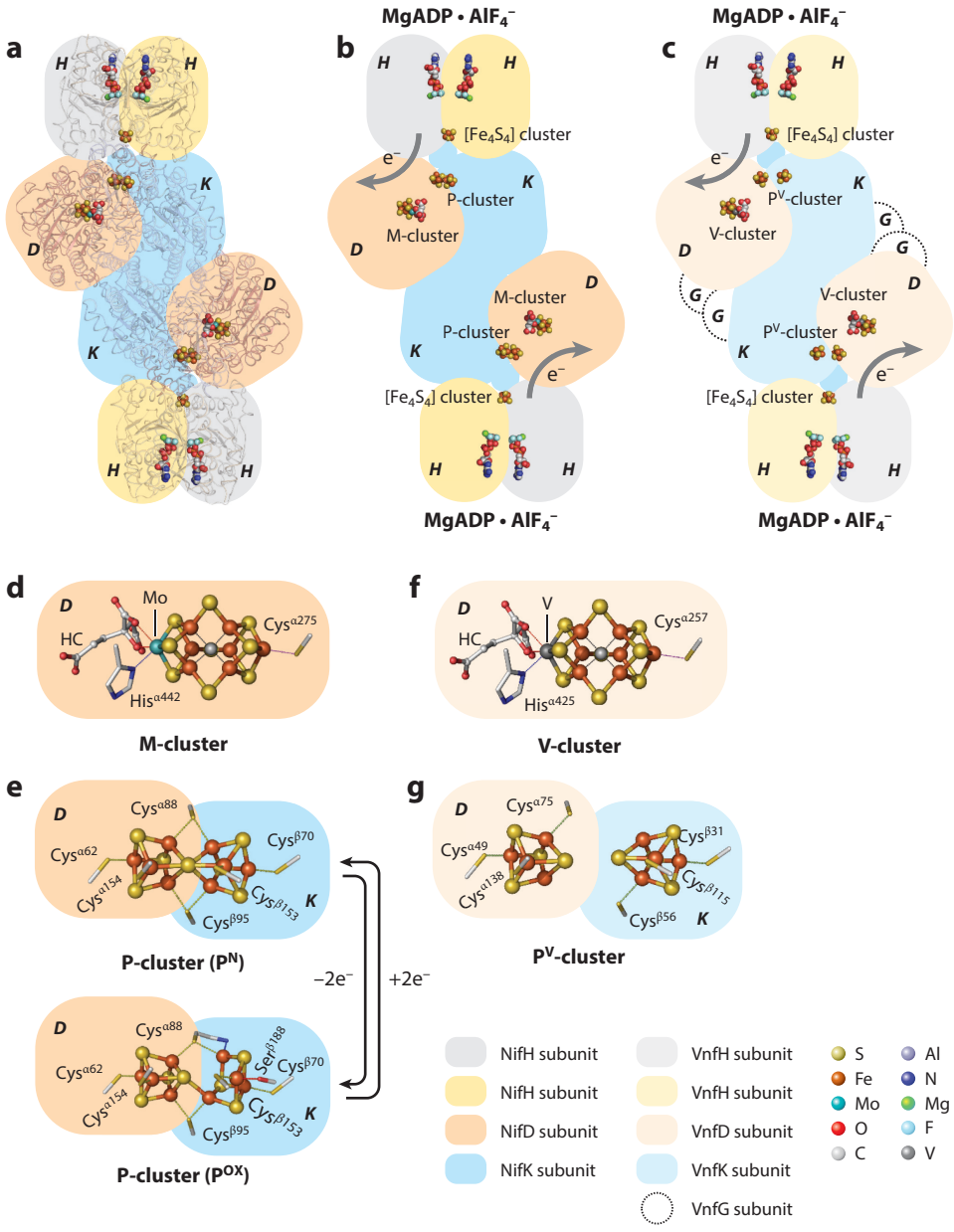

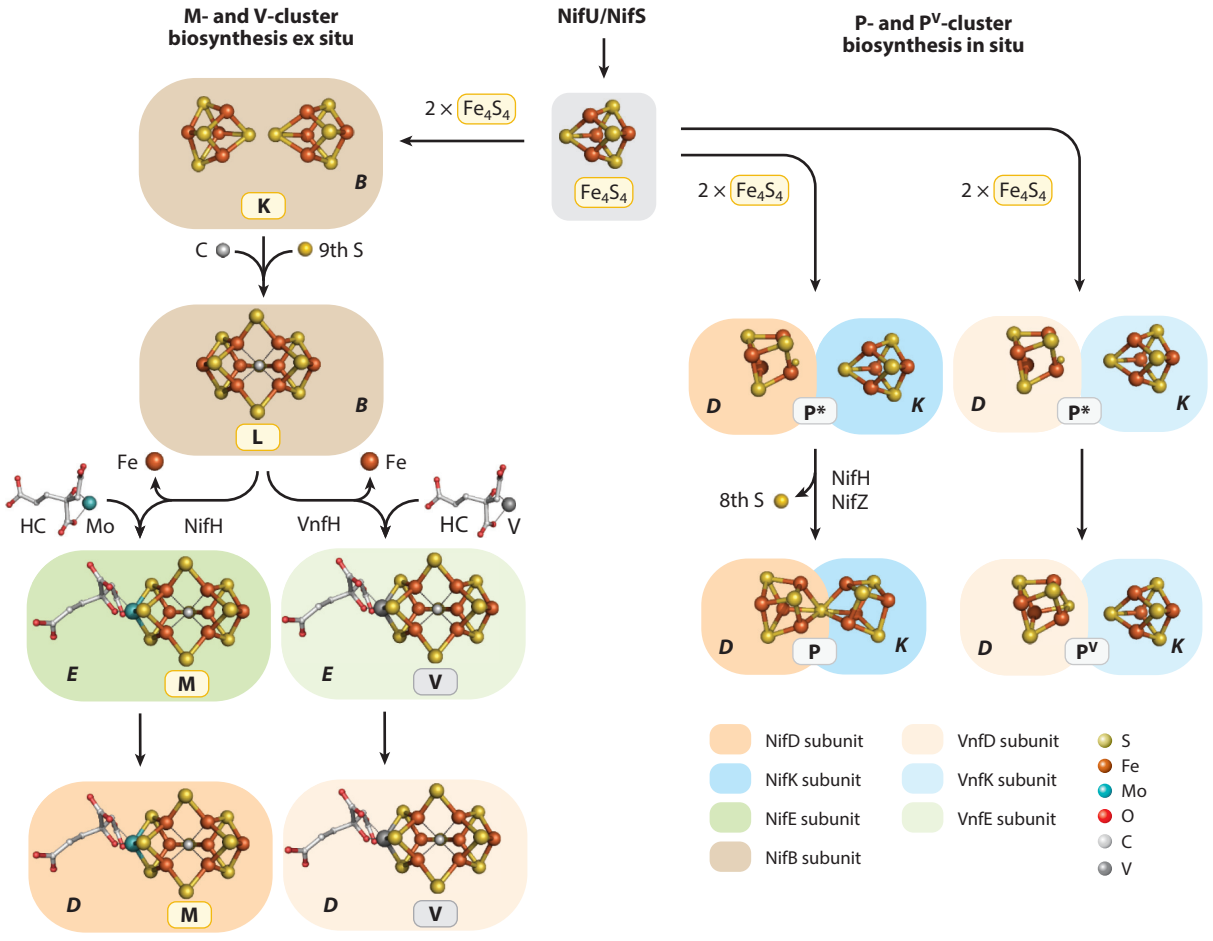

Figure 2

Flow diagrams of (*left*) the ex situ pathway of M- and V-cluster assembly and (*right*) the in situ pathway of P- and P^V-cluster assembly. Biosynthesis of all these clusters shares two common apparatuses, NifS and NifU, at the early stages of these assembly processes, where $[Fe_4S_4]$ units are generated as the building blocks for further construction of these clusters. Both pathways then use a pair of 4Fe units to form an 8Fe cluster; however, this step occurs on different proteins in these pathways. In the case of M- and V-cluster assembly, two $[Fe_4S_4]$ modules (K-cluster) are coupled into an $[Fe_8S_9]$ cluster (L-cluster) on NifB concomitantly with the radical *S*-adenosyl-L-methionine-dependent C insertion and the addition of the 9th S by an unknown mechanism. The L-cluster is further processed on NifEN into an M-cluster (a $[MoFe_7S_9C\text{-}HC]$ cluster) upon NifH-mediated insertion of Mo and HC, or on VnfEN into a V-cluster (likely a $[VFe_7S_9C\text{-}HC]$ cluster) upon VnfH-mediated insertion of V and HC. In the case of P-cluster assembly on NifDK, a pair of $[Fe_4S_4]$-like clusters (P*-cluster) is coupled into an $[Fe_8S_7]$ cluster (P-cluster) in a process that requires the actions of NifH and NifZ. In the case of the P^V-cluster on VnfDGK, however, it is possible that the coupling between an $[Fe_4S_4]$-like cluster pair either does not occur at all or proceeds only to a certain degree, as the P^V-cluster appears to closely resemble the P*-cluster in structure, based on biochemical and spectroscopic data (3, 6). All clusters are shown as ball-and-stick models, with the atoms colored as those in **Figure 1**. Only the subunits of the proteins housing the clusters are indicated in the figure. PYMOL (**https://www.pymol.org/**) was used to generate these structural models (Protein Data Bank identification numbers: 3U7Q, 1M1N, and 3PDI). Abbreviations: C, carbon; Fe, iron; HC, homocitrate; Mo, molybdenum; S, sulfur; V, vanadium.

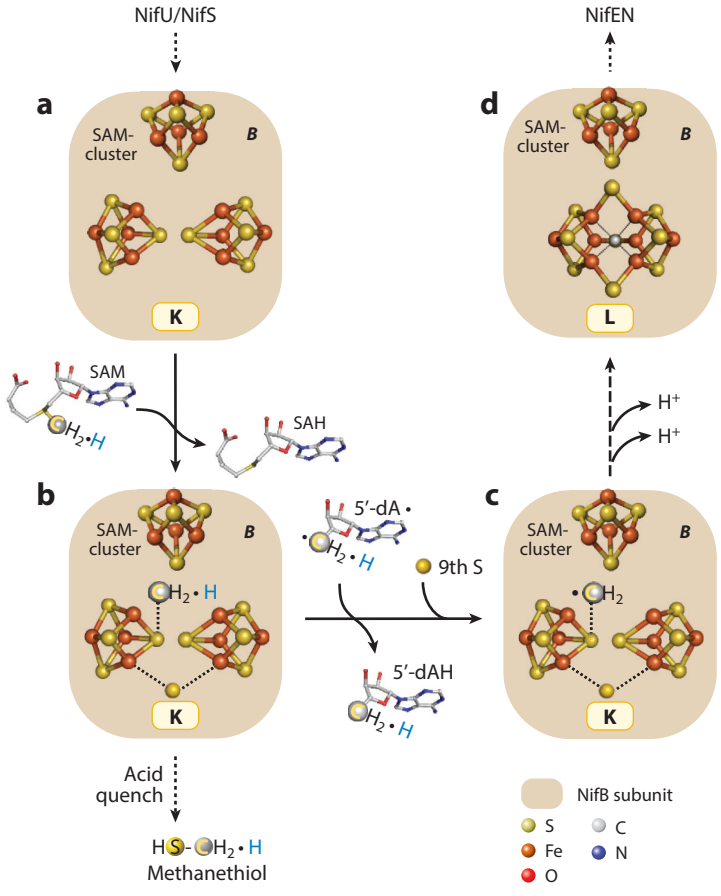

Figure 3

Schematic presentation of the formation of an L-cluster on NifB. (*a*) The combined action of NifS and NifU generates [Fe_4S_4] clusters, which are delivered to NifB and used to form the SAM-cluster and the two [Fe_4S_4] modules of the K-cluster on NifB. (*b*) A radical SAM-mediated process generates a SAM-derived methyl group that is transferred to an S atom of the K-cluster via an SN2-type mechanism. The methyl group that is attached to this labile S atom can be released as methanethiol upon acid quenching. (*c*) An S-bound methylene radical is formed upon hydrogen atom abstraction by 5′-dA• concomitant with the insertion of a 9th S into the K-cluster. (*d*) Continued deprotonation of the cluster-bound methylene radical eventually gives rise to an interstitial carbide atom concomitantly with the coupling and rearrangement of the cluster into an L-cluster. The L-cluster is subsequently transferred to NifEN for further maturation. All clusters and the SAM molecule are shown as ball-and-stick models, with the atoms colored as those in **Figure 1**. PYMOL (**https://www.pymol.org/**) was used to generate these structural models (Protein Data Bank identification number: 3PDI). Abbreviations: 5′-dA•, 5′-deoxyadenosyl radical; 5′-dAH, 5′-deoxyadenosine; S, sulfur; SAH, *S*-adenosyl-L-homocysteine; SAM, *S*-adenosyl-L-methionine.

an [Fe_8S_9C] cluster concomitantly with the radical SAM-dependent insertion of carbide (92–94) and the addition of a ninth sulfur (**Figure 3*b–d***).

The identification of the SAM cleavage products of NifB provided the initial insights into the mechanism of NifB (95, 96). In the presence of NifB, SAM is cleaved into two products: 5′-deoxyadenosine (5′-dA) and *S*-adenosyl-L-homocysteine (SAH) (**Figure 4*c***) (95). Upon substitution of [methyl-d_3] SAM for unlabeled SAM, deuterated 5′-dA (i.e., 5′-dAD) and unlabeled

5′-dA (i.e., 5′-dAH) are formed together with SAH as products of SAM cleavage (**Figure 4*d***) (95). These SAM cleavage and deuterium substitution patterns parallel those of the radical SAM RNA methyltransferases, RlmN and Cfr (97, 98), leading to an analogous proposal that NifB catalyzes an initial SN2-type methyl transfer from one equivalent of SAM to the protein (resulting in the formation of SAH) and a subsequent hydrogen abstraction of the methyl group by a 5′-deoxyadenosyl radical (5′-dA•) that is generated by homolytic cleavage of a second equivalent of SAM (resulting in the formation of 5′-dAH). Radiolabeling experiments have provided compelling evidence for this proposal, demonstrating that incubating NifB with [methyl-^{14}C] SAM

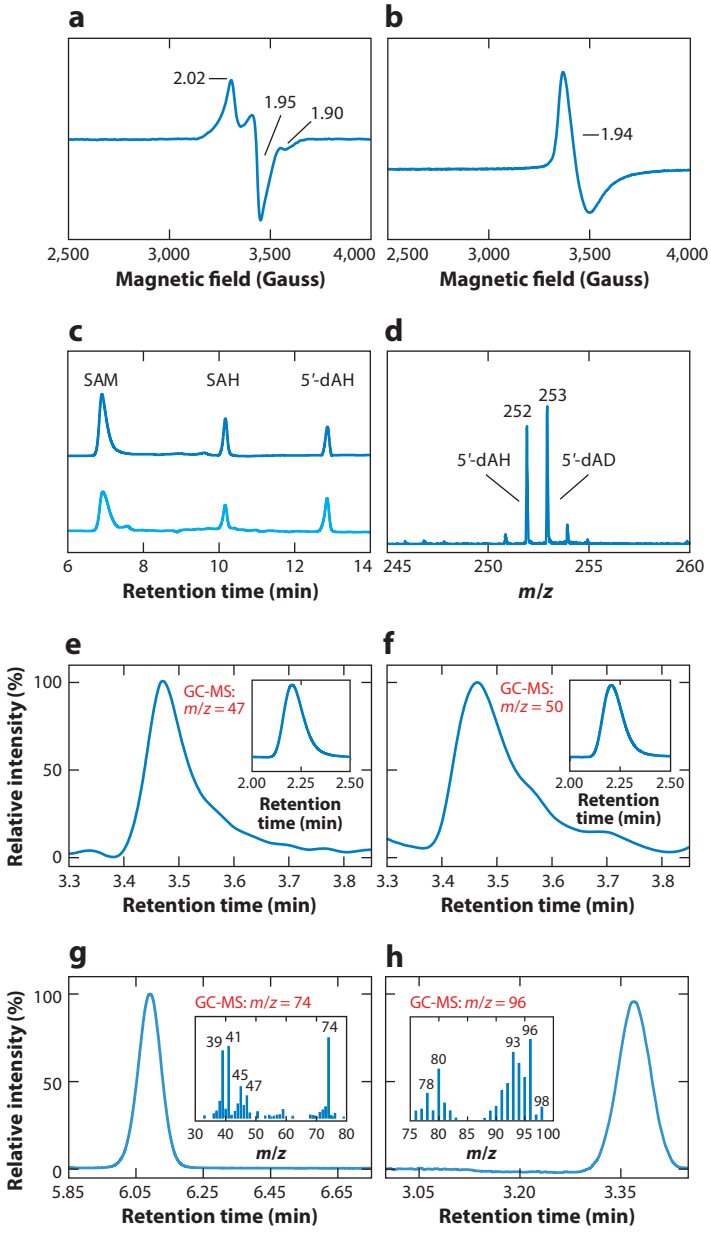

results in the accumulation of ^{14}C label in this protein, which can be further traced to the L-cluster upon extraction (95). The fact that the ^{14}C label is absent from the polypeptides of NifB supports the direct transfer of methyl to the K-cluster without going through a protein-bound carbon-intermediate step (95). More importantly, the observation that the ^{14}C label ends up in the L-cluster provides the definitive proof for carbon insertion occurring concomitantly with the coupling and rearrangement of the two 4Fe modules of the K-cluster into an 8Fe L-cluster.

A mechanism can be proposed for carbide insertion based on these observations, the early stage of which involves the direct transfer of the methyl group from SAM to a K-cluster-associated sulfur atom and the subsequent formation of a methylene radical upon abstraction of a hydrogen atom from this methyl group (**Figure 3*b*,*c***) (95). This proposal was proven correct by a recent study that used acid quenching, selenium (Se) labeling, and SAM analog experiments to determine the attachment of the methyl group and the sequence of events between methyl transfer and hydrogen abstraction (99). Acid treatment of a mixture containing NifB and either unlabeled SAM or [methyl-d_3] SAM results in the formation of methanethiol (CH_3SH) or methane-d_3-thiol (CD_3SH), suggesting that the SAM-derived methyl group is transferred to an acid-labile sulfur atom that is associated with the NifB-bound FeS cluster (**Figure 4*e*,*f***) (99). Upon substitution of Se for S in the NifB-associated FeS clusters, however, methylselenol (CH_3SeH) is generated as the product of acid quenching, further confirming that the S atom for methyl attachment indeed comes from an FeS cluster on NifB (**Figure 4*g***) (99). When NifB is incubated with allyl SAM, a SAM analog containing an allyl group (-CH-CH = CH_2) in place of a methyl group (-CH_3), SAH is formed as the sole product, suggesting that allyl transfer occurs without the accompanying hydrogen abstraction from the allyl group. Acid quenching of the mixture containing NifB and allyl SAM results in the formation of allylthiol (CH_2 = CH-CH-SH), providing compelling evidence

Figure 4

Biochemical and spectroscopic analyses of the conversion of a K-cluster to an L-cluster on NifB. (*a*) The K-cluster and the SAM-cluster collectively give rise to a SAM-responsive $S = 1/2$ signal at $g = 2.02$, 1.95, and 1.90 in the dithionite-reduced state, which disappears upon the addition of SAM concomitant with the appearance of (*b*) an L-cluster-specific $g = 1.94$ signal in the IDS-oxidized state, suggesting the conversion of a K-cluster to an L-cluster in this process. (*c*) The HPLC elution profile of the cleavage products of SAM (i.e., SAH and 5′-dAH) upon incubation with NifB and dithionite (*bottom trace*) is shown in comparison with the elution profiles of SAM, SAH, and 5′-dAH standards (*top trace*). (*d*) LC-MS analysis of the incubation mixture containing NifB and [methyl-d_3] SAM, showing the formation of 5′-dAD that results from abstraction of a hydrogen atom (labeled with deuterium) from the methyl group of SAM. (*e*,*f*) GC-MS (*inset*) and GC analyses of acid-quenched incubation mixtures containing NifB and either (*e*) SAM or (*f*) [methyl-d_3] SAM. The formation of methanethiol ($m/z = 47$) and methane-d_3-thiol ($m/z = 50$) upon acid treatment suggests the transfer of the SAM-derived methyl group to an acid-labile sulfur atom that is associated with the K-cluster. (*g*) GC-MS (*inset*) and GC analyses of acid-quenched incubation mixtures containing Fe- and Se-reconstituted NifB and SAM. The formation of methylselenol ($m/z = 74$) upon acid treatment confirms the transfer of the SAM-derived methyl group to an S atom (represented by Se) of the K-cluster. (*h*) GC-MS (*inset*) and GC analyses of acid-quenched incubation mixtures containing NifB and allyl SAM. The formation of allylthiol upon acid treatment ($m/z = 96$) suggests that methyl transfer (represented by allyl transfer) occurs prior to hydrogen abstraction, as allyl SAM is capable of undergoing allyl transfer without hydrogen abstraction when it is incubated with NifB. Note that a NifEN-B protein, in which NifB is fused with its immediate downstream assembly partner, NifEN, is used in these studies as a source of NifB. Abbreviations: Fe, iron; GC-MS, gas chromatography–mass spectrometry; HPLC, high-performance liquid chromatography; IDS, indigo disulfonate; LC-MS, liquid chromatography–mass spectrometry; S, sulfur; SAH, *S*-adenosyl-L-homocysteine; SAM, *S*-adenosyl-L-methionine; Se, selenium; *m*/*z*, mass-to-charge ratio.

that allyl transfer (which is analogous to methyl transfer) occurs independently of, and prior to, the hydrogen abstraction event (**Figure 4*b***) (99).

Details of the events following the early steps of carbide insertion are unclear. Nevertheless, the initial methyl transfer and hydrogen abstraction from the methyl group generate a K-cluster-associated carbon intermediate, which initiates the radical chemistry for the restructuring and coupling of the 4Fe units of the K-cluster into an 8Fe L-cluster. At the same time, the carbon intermediate undergoes additional deprotonation or dehydrogenation steps, or both, until a carbide ion is formed in the center of the L-cluster (**Figure 3*d***). To complete the stoichiometry of the L-cluster, there must be a concomitant insertion of a ninth sulfur, which could originate from SAM, given the documented ability of SAM to serve as a sulfur donor (92, 100). Alternatively, it could originate from a dangling sulfur atom attached to the K-cluster in an analogous manner to that observed in the cases of other radical SAM-dependent enzymes, such as RimO, MiaB, and HydG (101–103), or radical enzymes, such as (*R*)-2-hydroxyisocaproyl-CoA dehydratase (104). Clearly, further investigations are required to address these questions and elucidate the structural and mechanistic details of NifB.

Maturation of the 8Fe Core into a Cofactor

Upon formation, the 8Fe core (or the L-cluster) is transferred from NifB to the next assembly scaffold, where it is matured into a fully assembled cofactor (**Figure 5*a*,*b***). This step marks the branching of the biosynthetic pathways of the M- and V-clusters, moving on from NifB to either NifEN or VnfEN for the continuation of M- or V-cluster assembly (**Figure 2**).

NifEN shares a significant degree of sequence homology with NifDK, leading to the hypothesis that NifEN contains clusters analogous to the P-cluster and the M-cluster in NifDK (105). Although the P-cluster analog in NifEN was identified earlier as an [Fe_4S_4] cluster (106), the M-cluster analog was captured much later on NifEN when this protein was expressed in a *nifHDK*-deletion background, which allowed for the accumulation of an 8Fe precursor (i.e., the L-cluster) in the absence of NifH (an essential protein for L-cluster maturation) and NifDK (the downstream acceptor for M-cluster) (87, 90, 107). Fe K-edge X-ray absorption spectroscopy and extended X-ray absorption fine structure (XAS/EXAFS) analyses of both the NifEN-bound (90) and the NMF-extracted (89) L-clusters (**Figure 6*a***) revealed a core structure that was nearly indistinguishable from that of the M-cluster. Crystallographic studies of NifEN (88) provided further support for the EXAFS-derived model of the L-cluster, demonstrating an electron density in this cluster that was compatible in shape and extent with those of an [Fe_8S_9] structure. Biochemical (95) and Fe Kβ X-ray emission spectroscopy (91) analyses finalized the composition of the L-cluster, showing the presence of an interstitial carbide in this [Fe_8S_9C] cluster and establishing the formation of an all-iron core of the cofactor as a biosynthetic event preceding the insertion of Mo and homocitrate.

The conversion of the 8Fe L-cluster into a mature cofactor was achieved by incubating NifEN with NifH, magnesium (Mg)ATP, dithionite, molybdate (MoO_4^{2-}), and homocitrate, which resulted in a NifEN-bound form of the M-cluster (107–110) that was capable of reconstituting and activating the cofactor-deficient apo-NifDK (108–110). Maturation of the L-cluster into an M-cluster was reflected by the disappearance of the L-cluster-specific signal at $g = 1.94$ in the EPR spectrum of the IDS-oxidized NifEN (**Figure 6*c***) and the concurrent appearance of an M-cluster-like signal at $g = 4.45$, 3.96, and 3.60 in the EPR spectrum of the dithionite-reduced NifEN (**Figure 6*d***) (109, 110). Fe and Mo K-edge XAS/EXAFS analyses revealed a structure of the NifEN-bound M-cluster nearly identical to that of the NifDK-bound M-cluster (**Figure 6*b***), apart from a slightly asymmetric coordination of Mo that originated from a different ligand environment

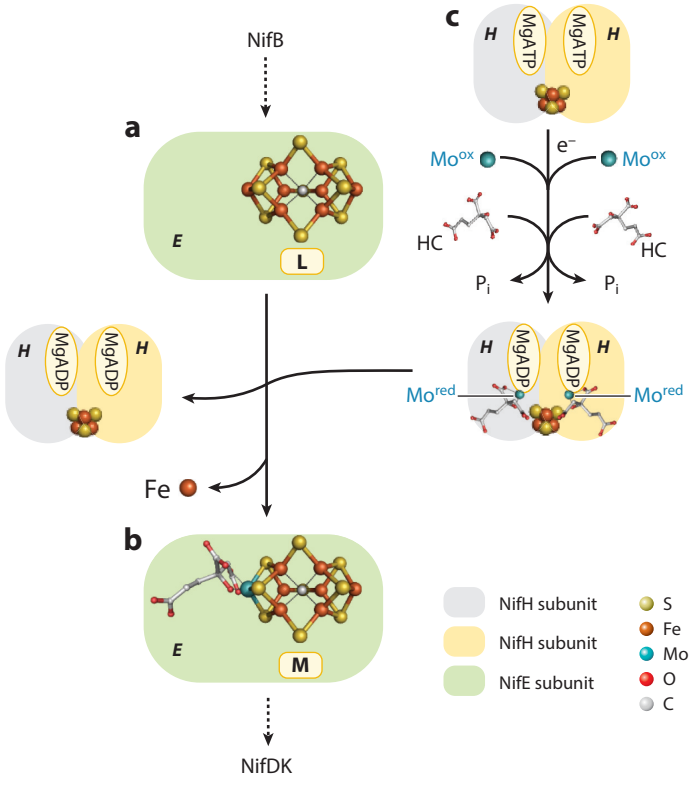

Figure 5

Schematic presentation of the formation of an M-cluster on NifEN. (*a*,*b*) NifEN hosts the conversion from an L- to an M-cluster upon the replacement of a terminal Fe atom by Mo and HC. (*c*) NifH serves as an ATP-dependent insertase of Mo and HC in this process. Mo and HC can be loaded on NifH in the presence of ATP and reductant. Mo is reduced in this process (indicated as $Mo^{ox} \rightarrow Mo^{red}$ in the figure), and it may enter NifH by attaching to the position that corresponds to the γ-phosphate of ATP upon ATP hydrolysis. Subsequently, the loaded NifH delivers Mo and HC to the NifEN-associated L-cluster and transforms it into a fully matured M-cluster. Following the completion of M-cluster assembly on NifEN, the M-cluster is delivered to its destined location in NifDK (*b*). The clusters are shown as ball-and-stick models, with the atoms colored as those in **Figure 1**. PYMOL (**https://www.pymol.org/**) was used to create the structural models in this figure (Protein Data Bank identification numbers: 3U7Q and 3PDI). For the purpose of simplicity, only the E (α)-subunit of NifEN is shown. Abbreviations: ADP, adenosine diphosphate; ATP, adenosine triphosphate; Fe, iron; HC, homocitrate; Mg, magnesium; Mo, molybdenum.

in NifEN (109, 110), whereas biochemical studies suggested a conformational rearrangement of NifEN upon conversion of the L-cluster to a mature M-cluster, which permitted complex formation between the M-cluster-bound NifEN and the cofactor-deficient apo-NifDK (111). This suggestion was further supported by the crystallographic analysis of NifEN, which revealed an unusual, nearly surface-exposed location of the L-cluster instead of the predicted M-cluster site buried within the α-subunit of NifEN (88). This observation has led to the proposal that the surface location of the L-cluster permits the easy access of Mo and homocitrate for the maturation of this cluster, which subsequently triggers a conformational change of NifEN that relocates the matured M-cluster from the surface of the protein to its binding site within the protein (80, 81, 83, 88).

The role of NifH in M-cluster maturation was further explored by re-isolating NifH after incubating this protein with NifEN, MgATP, dithionite, molybdate (MoO_4^{2-}), and homocitrate

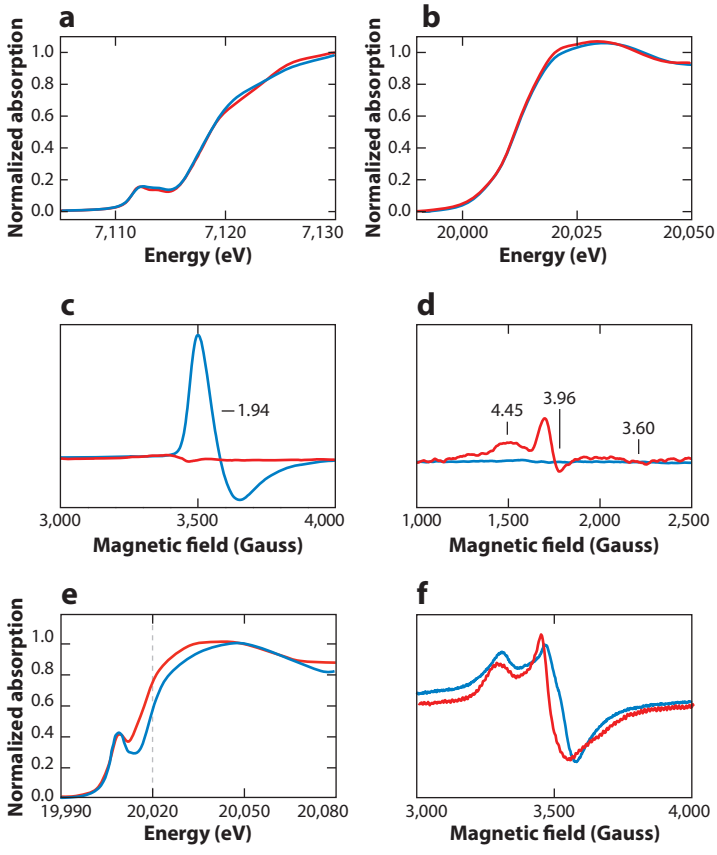

Figure 6

Biochemical and spectroscopic analyses of the conversion of an L-cluster to an M-cluster on NifEN. (*a*) Iron (Fe) K-edge X-ray absorption spectroscopy (XAS) spectra of the L-cluster (*blue*) and the M-cluster (*red*) in the solvent-extracted state and (*b*) molybdenum (Mo) K-edge XAS spectra of the M-clusters on NifEN (*blue*) and NifDK (*red*). (*c*) The L-cluster can be recognized by a unique $g = 1.94$ signal in the indigo disulfonate-oxidized state (*blue*) that disappears upon M-cluster maturation (*red*). (*d*) Upon maturation, the M-cluster on NifEN displays a small M-cluster-like electron paramagnetic resonance (EPR) signal at $g = 4.45$, 3.96, and 3.60 in the dithionite-reduced state (*red*) that is not observed in the case of the L-cluster (*blue*). (*e*) Normalized Mo K-edge XAS spectra of molybdate (*blue*) and the Mo–homocitrate-loaded NifH (*red*). A dashed reference line was drawn at 20,020 eV for comparison of edge positions. (*f*) EPR spectra of the magnesium–adenosine triphosphate (MgATP)-bound NifH (*blue*) and the Mo–homocitrate-loaded NifH (*red*).

(108). Biochemical experiments indicated that the re-isolated NifH was loaded with Mo and homocitrate (**Figure 5*c***), and, therefore, could directly serve as a donor of these two missing components for the maturation of the L-cluster on NifEN (108). Further, these experiments revealed a strict dependence of NifH on ATP hydrolysis and redox potentials to carry out this function, as well as an interesting, obligate comobilization of Mo and homocitrate by this protein (108–111). Mo K-edge XAS analysis (**Figure 6*e***) suggested a change in the oxidation state or ligation pattern, or both, of the Mo species upon binding to NifH (108), whereas EPR analysis revealed an intermediary line shape of the loaded NifH (**Figure 6*f***) that was between those of the adenosine diphosphate (ADP)- and ATP-bound forms of NifH (108), which coincided with the

previously observed binding of Mo at a position corresponding to the γ-phosphate of ATP in the first crystal structure of the ADP-bound conformation of NifH (112). Although the exact mode of action of NifH in this process awaits further investigation, these observations firmly establish this protein as an essential ATP-dependent Mo–homocitrate insertase in the process of M-cluster maturation.

Compared with the amount of information acquired about how an 8Fe core (or L-cluster) is converted to an M-cluster on NifEN, little is known about how the same 8Fe core is matured into a V-cluster on VnfEN. However, given the sequence homology between NifEN and VnfEN (NifE/VnfE, 82%; NifN/VnfN, 67%), as well as that between NifH and VnfH (95%) (**Figure 7*a*,*b***), the same mechanism could be used to perform this function, although the maturation of an 8Fe core into a V-cluster is facilitated by VnfH-mediated insertion of V and homocitrate in this case. Moreover, the presence of two conserved ligands ($Cys^{\alpha 15}$ and $Cys^{\alpha 25}$) (**Figure 7*b***) that potentially ligate the L-cluster at the surface of VnfEN, along with the two conserved ligands ($Cys^{\alpha 250}$ and $Asn^{\alpha 418}$) (**Figure 7*b***) that potentially ligate the V-cluster at the cofactor-binding site within VnfEN, could enable the transfer of the V-cluster upon maturation from the surface to the inside of the protein in the same manner as that proposed for NifEN. It is interesting that a heterologous maturation system using NifH to insert V (in VO_4^{3-}) and homocitrate into the NifEN-bound L-cluster permitted only a partial conversion of the L-cluster into a cluster species that had low V occupancy and was incapable of reconstituting and activating apo-NifDK (113). This observation points to a number of factors that could impact the specificity of core maturation and transfer, such as the redox potential of the NifH- or VnfH-associated $[Fe_4S_4]$ cluster that is required for the specific and efficient loading of a certain heterometal, the particular conformational rearrangement of NifEN or VnfEN that is induced upon insertion of a specific heterometal, and the proper docking of NifEN or VnfEN on NifDK or VnfDK that is required to deliver a specific cofactor to its target binding site.

Delivery of the Cofactor to Its Target Binding Site

The completion of cofactor assembly signals the transfer of the cofactor from the assembly scaffold to its target binding site (**Figure 5*b***). In the case of M-cluster assembly, this signal is conveyed by a conformational change of NifEN upon M-cluster maturation, which allows the subsequent complex formation between NifEN and apo-NifDK (111). The M-cluster is then delivered within this complex from its assembly site in NifEN to its target binding site in NifDK via direct protein–protein interactions, as the reconstitution of cofactor-deficient apo-NifDK can be readily accomplished upon incubation of this protein with the M-cluster-bound NifEN (109, 110).

Sequence alignment sheds light on the underlying principle of the direct cluster transfer mechanism between NifEN and NifDK, revealing the absence of certain residues from the sequence of NifEN that either provide a covalent ligand to the M-cluster or tightly pack the M-cluster within the polypeptide matrix of NifDK (85). Such a discrepancy could very well facilitate a diffusion of the M-cluster from its transient binding site in NifEN (the low-affinity site) to the target binding site in NifDK (the high-affinity site) (80, 111). Indeed, the analogous cluster-binding sites in NifEN and NifDK can be identified by comparing the crystal structures of the L-cluster-bound NifEN, the cofactor-replete holo-NifDK, and the cofactor-deficient apo-NifDK (**Figure 8*a***) (17, 18, 86, 88). More importantly, the structural comparison between these proteins reveals the presence of homologous cofactor-insertion paths in NifEN and NifDK, which extend from the protein surfaces to the cofactor-binding sites within the respective proteins (**Figure 8*b***). In apo-NifDK, this cofactor-insertion path is lined with positively charged residues (**Figure 7*c***), which could facilitate the insertion of the negatively charged M-cluster through electrostatic interactions (80–86). By

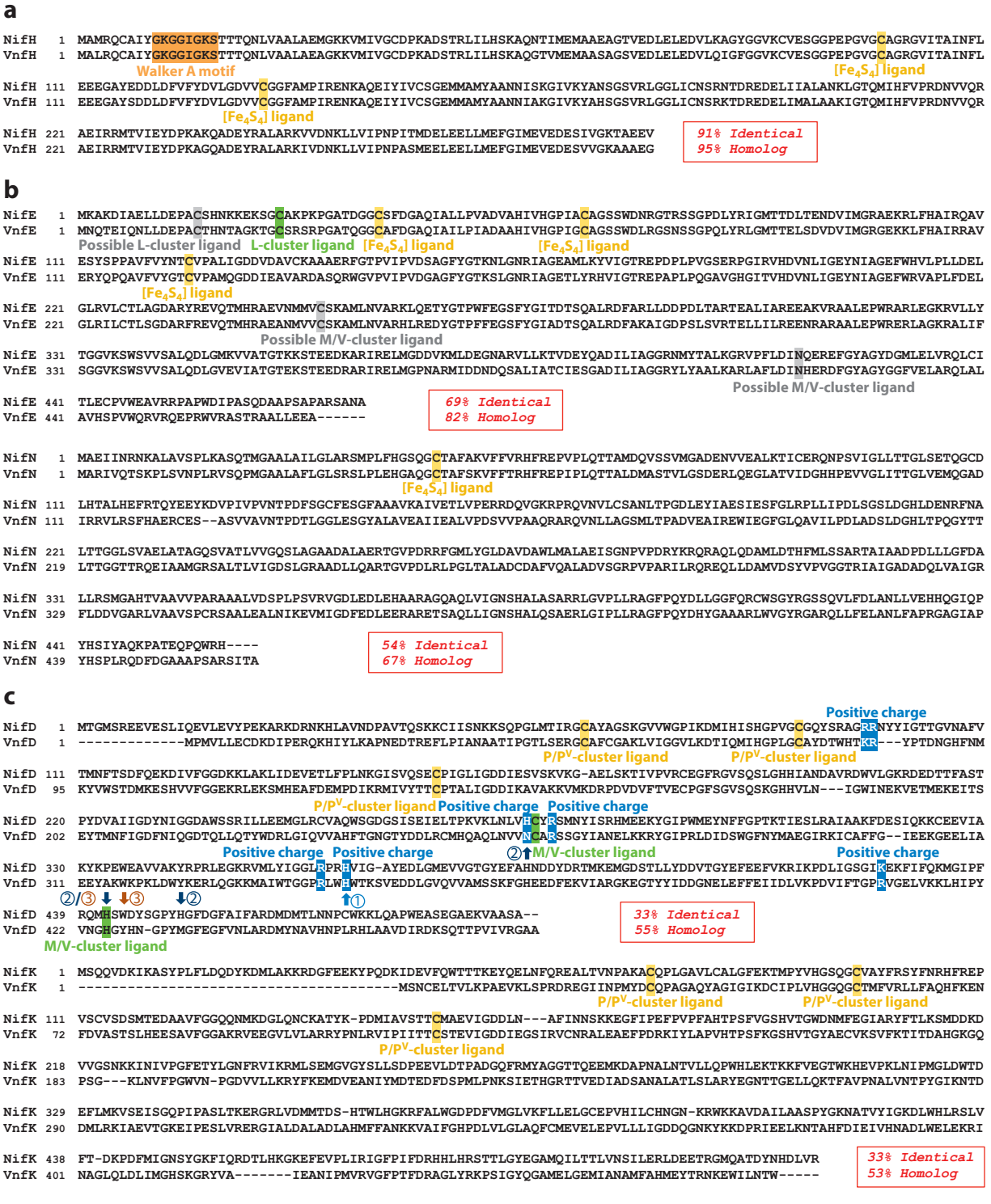
a
NifH 1 MAMRQCAIYGKGGIGKSTTTQNLVAALAEMGKKVMIVGCDPKADSTRLILHSKAQNTIMEMAAEAGTVEDLELEDVLKAGYGGVKCVESGGPEPGVGCAGRGVITAINFL
VnfH 1 MALRQCAIYGKGGIGKSTTTQNLVAALAEAGKKVMIVGCDPKADSTRLILHSKAQGTVMEMAASAGSVEDLELEDVLQIGFGGVKCVESGGPEPGVGCAGRGVITAINFL
Walker A motif
[Fe4S4] ligand
NifH 111 EEEGAYEDDLDFVFYDVLGDVVCGGFAMPIRENKAQEIYIVCSGEMMAMYAANNISKGIVKYANSGSVRLGGLICNSRNTDREDELIIALANKLGTQMIHFVPRDNVVQR
VnfH 111 EEEGAYSDDLDFVFYDVLGDVVCGGFAMPIRENKAQEIYIVCSGEMMAMYAANNIAKGIVKYAHSGSVRLGGLICNSRKTDREDELIMALAAKIGTQMIHFVPRDNVVQR
[Fe4S4] ligand
NifH 221 AEIRRMTVIEYDPKAKQADEYRALARKVVDNKLLVIPNPITMDELEELLMEFGIMEVEDESIVGKTAEEV
VnfH 221 AEIRRMTVIEYDPKAGQADEYRALARKIVDNKLLVIPNPASMEELEELLMEFGIMEVEDESVVGKAAAEG
91% Identical
95% Homolog
b
NifE 1 MKAKDIAELLDEPACSHNKKEKSGCAKPKPGATDGGCSFDGAQIALLPVADVAHIVHGPIACAGSSWDNRGTRSSGPDLYRIGMTTDLTENDVIMGRAEKRLFHAIRQAV
VnfE 1 MNQTEIQNLLDEPACTHNTAGKTCSRSRPGATQGGCAFDGAQIAILPIADAAHIVHGPIGCAGSSWDLRGSNSSGPQLYRLGMTTELSDVDVIMGRGEKKLFHAIRRAV
Possible L-cluster ligand
L-cluster ligand
[Fe4S4] ligand
[Fe4S4] ligand
NifE 111 ESYSPPAVFVYNTCVPALIGDDVDAVCKAAAERFGTPVIPVDSAGFYGTKNLGNRIAGEAMLKYVIGTREPDPLPVGSERPGIRVHDVNLIGEYNIAGEFWHVLPLLDEL
VnfE 111 ERYQPQAVFVYGTCVPAMQGDDIEAVARDASQRWGVPVIPVDGAGFYGTKSLGNRIAGETLYRHVIGTREPAPLPQGAVGHGITVHDVNLIGEYNIAGEFWRVAPLFDEL
[Fe4S4] ligand
NifE 221 GLRVLCTLAGDARYREVQTMHRAEVNMMVCSKAMLNVARKLQETYGTPWFEGSFYGITDTSQALRDFARLLDDPDLTARTEALIAREEAKVRAALEPWRARLEGKRVLLY
VnfE 221 GLRILCTLSGDARFREVQTMHRAEANMVVCSKAMLNVARHLREDYGTPFFEGSFYGIADTSQALRDFAKAIGDPSLSVRTELLILREENRARAALEPWRERLAGKRALIF
Possible M/V-cluster ligand
NifE 331 TGGVKSWSVVSALQDLGMKVVATGTKKSTEEDKARIRELMGDDVKMLDEGNARVLLKTVDEYQADILIAGGRNMYTALKGRVPFLDINQEREFGYAGYDGMLELVRQLCI
VnfE 331 SGGVKSWSVVSALQDLGVEVIATGTEKSTEEDRARIRELMGPNARMIDDNDQSALIATCIESGADILIAGGRYLYAALKARLAFLDINHERDFGYAGYGGFVELARQLAL
Possible M/V-cluster ligand
NifE 441 TLECPVWEAVRRPAPWDIPASQDAAPSAPARSANA
VnfE 441 AVHSPVWQRVRQEPRWVRASTRAALLEEA------
69% Identical
82% Homolog
NifN 1 MAEIINRNKALAVSPLKASQTMGAALAILGLARSMPLFHGSQGCTAFAKVFFVRHFREPVPLQTTAMDQVSSVMGADENVVEALKTICERQNPSVIGLLTTGLSETQGCD
VnfN 1 MARIVQTSKPLSVNPLRVSQPMGAALAFLGLSRSLPLEHGAQGCTAFSKVFFTRHFREPIPLQTTALDMASTVLGSDERLQEGLATVIDGHHPEVVGLITTGLVEMQGAD
[Fe4S4] ligand
NifN 111 LHTALHEFRTQYEEYKDVPIVPVNTPDFSGCFESGFAAAVKAIVETLVPERRDQVGKRPRQVNVLCSANLTPGDLEYIAESIESFGLRPLLIPDLSGSLDGHLDENRFNA
VnfN 111 IRRVLRSFHAERCES--ASVVAVNTPDTLGGLESGYALAVEAIIEALVPDSVVPAAQRARQVNLLAGSMLTPADVEAIREWIEGFGLQAVILPDLADSLDGHLTPQGYTT
NifN 221 LTTGGLSVAELATAGQSVATLVVGQSLAGAADALAERTGVPDRRFGMLYGLDAVDAWLMALAEISGNPVPDRYKRQRAQLQDAMLDTHFMLSSARTAIAADPDLLLGFDA
VnfN 219 LTTGGTTRQEIAAMGRSALTLVIGDSLGRAADLLQARTGVPDLRLPGLTALADCDAFVQALADVSGRPVPARILRQREQLLDAMVDSYVPVGGTRIAIGADADQLVAIGR
NifN 331 LLRSMGAHTVAAVVPARAAALVDSPLPSVRVGDLEDLEHAARAGQAQLVIGNSHALASARRLGVPLLRAGFPQYDLLGGFQRCWSGYRGSSQVLFDLANLLVEHHQGIQP
VnfN 329 FLDDVGARLVAAVSPCRSAALEALNIKEVMIGDFEDLEERARETSAQLLIGNSHALQSAERLGIPLLRAGFPQYDHYGAAARLWVGYRGARQLLFELANLFAPRGAGIAP
NifN 441 YHSIYAQKPATEQPQWRH----
VnfN 439 YHSPLRQDFDGAAAPSARSITA
54% Identical
67% Homolog
c
Positive charge
NifD 1 MTGMSREEVESLIQEVLEVYPEKARKDRNKHLAVNDPAVTQSKKCIISNKKSQPGLMTIRGCAYAGSKGVVWGPIKDMIHISHGPVGCGQYSRAGRRNYYIGTTGVNAFV
VnfD 1 ------------MPMVLLECDKDIPERQKHIYLKAPNEDTREFLPIANAATIPGTLSERGCAFCGAKLVIGGVLKDTIQMIHGPLGCAYDTWHTKR---YPTDNGHFNM
P/PV-cluster ligand
P/PV-cluster ligand
NifD 111 TMNFTSDFQEKDIVFGGDKKLAKLIDEVETLFPLNKGISVQSECPIGLIGDDIESVSKVKG-AELSKTIVPVRCEGFRGVSQSLGHHIANDAVRDWVLGKRDEDTTFAST
VnfD 95 KYVWSTDMKESHVVFGGEKRLEKSMHEAFDEMPDIKRMIVYTTCPTALIGDDIKAVAKKVMKDRPDVDVFTVECPGFSGVSQSKGHHVLN---IGWINEKVETMEKEITS
P/PV-cluster ligand
Positive charge
Positive charge
NifD 220 PYDVAIIGDYNIGGDAWSSRILLEEMGLRCVAQWSGDGSISEIELTPKVKLNLVHCYRSMNYISRHMEEKYGIPWMEYNFFGPTKTIESLRAIAAKFDESIQKKCEEVIA
VnfD 202 EYTMNFIGDFNIQGDTQLLQTYWDRLGIQVVAHFTGNGTYDDLRCMHQAQLNVVNCARSSGYIANELKKRYGIPRLDIDSWGFNYMAEGIRKICAFFG--IEEKGEELIA
Positive charge
Positive charge
M/V-cluster ligand
Positive charge
NifD 330 KYKPEWEAVVAKYRPRLEGKRVMLYIGGLRPRHVIG-AYEDLGMEVVGTGYEFAHNDDYDRTMKEMGDSTLLYDDVTGYEFEEFVKRIKPDLIGSGIKEKFIFQKMGIPF
VnfD 311 EEYAKWKPKLDWYKERLQGKKMAIWTGGPRLWHWTKSVEDDLGVQVVAMSSKFGHEEDFEKVIARGKEGTYYIDDGNELEFFEIIDLVKPDVIFTGPRVGELVKKLHIPY
②/③ ③ ② ①
NifD 439 RQMHSWDYSGPYHGFDGFAIFARDMDMTLNNPCWKKLQAPWEASEGAEKVAASA--
VnfD 422 VNGHGYHN-GPYMGFEGFVNLARDMYNAVHNPLRHLAAVDIRDKSQTTPVIVRGAA
33% Identical
55% Homolog
M/V-cluster ligand
NifK 1 MSQQVDKIKASYPLFLDQDYKDMLAKKRDGFEEKYPQDKIDEVFQWTTTKEYQELNFQREALTVNPAKACQPLGAVLCALGFEKTMPYVHGSQGCVAYFRSYFNRHFREP
VnfK 1 --MSNCELTVLKPAEVKLSPRDREGIINPMYDCQPAGAQYAGIGIKDCIPLVHGGQGCTMFVRLLFAQHFKEN
P/PV-cluster ligand
P/PV-cluster ligand
NifK 111 VSCVSDSMTEDAAVFGGQQNMKDGLQNCKATYK-PDMIAVSTTCMAEVIGDDLN---AFINNSKKEGFIPEFPVPFAHTPSFVGSHVTGWDNMFEGIARYFTLKSMDDKD
VnfK 72 FDVASTSLHEESAVFGGAKRVEEGVLVLARRYPNLRVIPIITTCSTEVIGDDIEGSIRVCNRALEAEFPDRKIYLAPVHTPSFKGSHVTGYAECVKSVFKTITDAHGKGQ
P/PV-cluster ligand
NifK 218 VVGSNKKINIVPGFETYLGNFRVIKRMLSEMGVGYSLLSDPEEVLDTPADGQFRMYAGGTTQEEMKDAPNALNTVLLQPWHLEKTKKFVEGTWKHEVPKLNIPMGLDWTD
VnfK 183 PSG---KLNVFPGWVN-PGDVVLLKRYFKEMDVEANIYMDTEDFDSPMLPNKSIETHGRTTVEDIADSANALATLSLARYEGNTTGELLQKTFAVPNALVNTPYGIKNTD
NifK 329 EFLMKVSEISGQPIPASLTKERGRLVDMMTDS-HTWLHGKRFALWGDPDFVMGLVKFLLELGCEPVHILCHNGN-KRWKKAVDAILAASPYGKNATVYIGKDLWHLRSLV
VnfK 290 DMLRKIAEVTGKEIPESLVRERGIALDALADLAHMFFANKKVAIFGHPDLVLGLAQFCMEVELEPVLLLIGDDQGNKYKKDPRIEELKNTAHFDIEIVHNADLWELEKRI
NifK 438 FT-DKPDFMIGNSYGKFIQRDTLHKGKEFEVPLIRIGFPIFDRHHLHRSTTLGYEGAMQILTTLVNSILERLDEETRGMQATDYNHDLVR
VnfK 401 NAGLQLDLIMGHSKGRYVA-------IEANIPMVRVGFPTFDRAGLYRKPSIGYQGAMELGEMIANAMFAHMEYTRNKEWILNTW-----
33% Identical
53% Homolog

analogy, the cofactor-insertion path in apo-NifEN would allow the relocation of the M-cluster from the protein surface to the cofactor-binding site within the protein upon maturation, inducing a conformational change of NifEN that is required for the docking of NifEN on apo-NifDK and the subsequent transfer of the cofactor to its final binding site in NifDK (111).

Based on this observation, a common pathway for cofactor insertion can be proposed for NifEN and NifDK (**Figure 9*a***), which consists of an apo conformation with an open insertion path, an intermediary conformation with the cofactor attached at the entrance of the path, and a holo conformation with the cofactor inserted at its binding site. The two pathways are linked by protein–protein interactions between NifEN and NifDK, which permit the release of the M-cluster from its transient binding site in NifEN back to the surface of the protein and the subsequent relay of the M-cluster from NifEN to the surface of NifDK through the coordinated actions of cysteinyl ligands, such as the $Cys^{\alpha 25}$ in NifEN and the corresponding $Cys^{\alpha 45}$ in NifDK (81, 83, 88). The M-cluster then interacts with a number of NifDK residues along the insertion path en route to its target binding site in this protein (**Figure 9*b***) (86). Among these residues, $His^{\alpha 362}$ resides in a so-called lid loop and potentially serves as a transient ligand for the M-cluster at the entrance of the insertion path. Additionally, $His^{\alpha 274}$, $His^{\alpha 442}$, and $His^{\alpha 451}$ form a His-triad that provides an intermediary docking point for the M-cluster halfway down the insertion path. Finally, $His^{\alpha 442}$ and $Trp^{\alpha 444}$ consist of a switch/lock that secures the M-cluster at its binding site by the bulky side-chain of $Trp^{\alpha 444}$ upon switching position with $His^{\alpha 442}$. Mutational analyses have provided strong support for the proposed roles of these residues in cofactor insertion (114–116), and small-angle X-ray scattering analyses have further revealed a more compacted conformation of NifDK upon incorporation of the cofactor, showing a more extended conformation of apo-NifDK [radius of gyration (R_g) = 42.4 Å] relative to that of holo-NifDK (R_g = 40.2 Å) (117). Such a conformational rearrangement signifies the completion of the assembly process of the M-cluster, closing up the insertion path and burying the M-cluster at a location that is approximately 10 Å below the surface of NifDK (**Figure 9*a***).

The final step of V-cluster assembly likely employs the same strategy as that of the M-cluster, which involves complex formation between VnfEN and VnfDGK upon V-cluster maturation, and the subsequent delivery of the V-cluster from VnfEN to its binding site in VnfDGK. This argument is supported by the overall sequence homology between VnfEN and NifEN (see Maturation of the 8Fe Core into a Cofactor), as well as that between VnfDGK and NifDK (VnfD/NifD, 55%; VnfK/NifK, 53%) (**Figure 7*c***). The insertion of the V-cluster into VnfDGK may also occur via a positively charged insertion path, particularly given that most of the positive residues lining

Figure 7

Amino acid sequence alignment of Nif and Vnf proteins of *Azotobacter vinelandii*. (*a*) Sequence alignment between NifH and VnfH. The two ligands of the [Fe_4S_4] cluster (*yellow*) and the Walker A motif of the adenosine triphosphate (ATP)-binding site (*orange*) are strictly conserved in both proteins. (*b*) Sequence alignments (*top*) between NifE and VnfE and (*bottom*) between NifN and VnfN. The four ligands of the [Fe_4S_4] cluster (*yellow*) are strictly conserved in the respective E (α)- and N (β)-subunits. In addition, the L-cluster ligand that has been identified (*green*) and proposed (*gray*) based on the crystal structure of NifEN, as well as the two M-cluster ligands (*gray*), are conserved in the E (α)-subunits. (*c*) Sequence alignments (*top*) between NifD and VnfD and (*bottom*) between NifK and VnfK. All six P-cluster ligands (*yellow*) are conserved in the respective D (α)- and K (α)-subunits, and the two M-cluster ligands (*green*) are conserved in the D (α)-subunits. Seven positively charged residues along the M-cluster insertion funnel (*blue*) are conserved in the D (α)-subunits. The lid-loop residue $His^{\alpha 362}$ (①) and the switch/lock residues $His^{\alpha 442}$ and $Trp^{\alpha 444}$ (③) are either conserved or replaced by similar amino acids, and two of the three His-triad residues ($His^{\alpha 274}$ and $His^{\alpha 442}$) (②) are conserved in the D (α)-subunits. The sequences were aligned using the program CLUSTALW (**http://www.genome.jp/tools/clustalw/**). The homology and identity between these sequences are indicated in the figure.

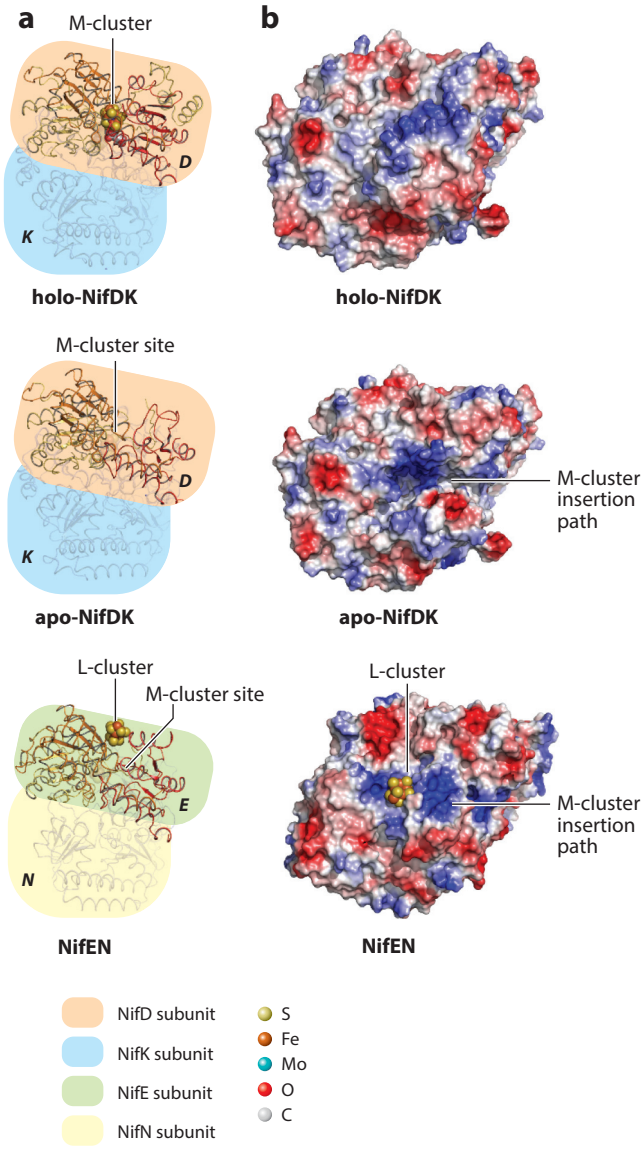

Figure 8

Structural conformations of NifEN and NifDK. (*a*) Schematic presentations of (*top*) holo-NifDK, (*middle*) apo-NifDK, and (*bottom*) NifEN. Structures of the αβ-dimers of holo-NifDK, apo-NifDK, and NifEN are shown as ribbon diagrams in the foreground, with the locations of the M-cluster sites, as well as the locations of the L- and M-clusters, highlighted in these proteins. All clusters are shown as space-filling models, with the atoms colored as those in **Figure 1**. The $[Fe_4S_4]$ cluster (the P-cluster equivalent) in NifEN and the P-cluster in NifDK are rendered transparent in the background. (*b*) Surface presentations of (*top*) holo-NifDK, (*middle*) apo-NifDK, and (*bottom*) NifEN. Electrostatic surface potentials of the αβ-dimers of holo-NifDK, apo-NifDK, and NifEN are shown, with the locations of insertion paths highlighted in these proteins. Negative and positive surface potentials are colored, respectively, red and blue. PYMOL (**https://www.pymol.org/**) was used to generate this figure (Protein Data Bank identification numbers: 1L5H, 3PDI, and 1M1N).

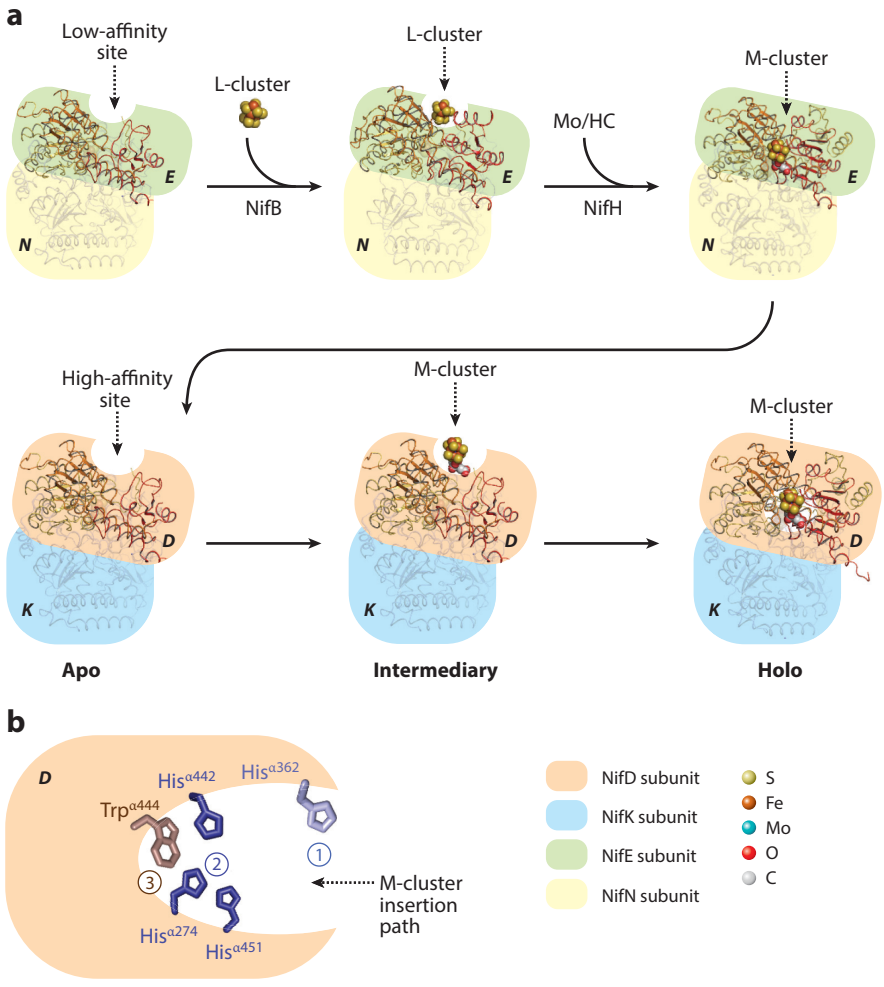

Figure 9

Transfer of the M-cluster between NifEN and NifDK. (*a*) NifEN and NifDK share a common cluster-insertion mechanism, in which three conformations appear sequentially: an apo conformation containing a cluster-insertion path; an intermediary conformation, which occurs upon the docking of the cluster at the entrance of the path; and a holo conformation, which occurs following the insertion of the cluster along the path into its binding site. The biosynthetic events on NifEN and NifDK are connected via complex formation and cluster transfer between the two proteins. Presentations of holo-NifDK, apo-NifDK, and the intermediary conformation of NifEN were generated as described in **Figure 7*a***, and presentations of holo-NifEN, apo-NifEN, and the intermediary conformation of NifDK were generated using the structural conformations corresponding to the proposed conformations of these proteins. (*b*) Close-up of the M-cluster insertion path leading to the high-affinity site in apo-NifDK. Some key residues for M-cluster insertion can be found along a positively charged insertion path that extends from the surface of the protein to the cluster-binding site within the protein. These residues include ① the lid-loop residue, His$^{\alpha 362}$, which may provide the first docking point for the M-cluster at the entrance of the insertion path; ② the His-triad residues, His$^{\alpha 274}$, His$^{\alpha 442}$, and His$^{\alpha 451}$, which may provide an intermediary docking point for the M-cluster halfway down the path; and ③ the switch/lock residues, His$^{\alpha 442}$ and Trp$^{\alpha 444}$, which may secure the M-cluster at its target binding site by the bulky side chain of Trp$^{\alpha 444}$ through a switch of the relative positions of Trp$^{\alpha 444}$ and His$^{\alpha 442}$. Abbreviations: HC, homocitrate; Mo, molybdenum.

the insertion path in NifDK—including Lys$^{\alpha 426}$, Arg$^{\alpha 96}$, Arg$^{\alpha 97}$, Arg$^{\alpha 277}$, Arg$^{\alpha 359}$, His$^{\alpha 274}$, and His$^{\alpha 362}$—are either conserved or similarly replaced (i.e., through a substitution of Arg for Lys, or vice versa) in VnfDGK (**Figure 7*c***). Moreover, residues in the three key regions along the insertion path in NifDK—namely, the lid-loop residue (Arg$^{\alpha 362}$), the His-triad (His$^{\alpha 274}$, His$^{\alpha 442}$, and His$^{\alpha 451}$), and the switch/lock (His$^{\alpha 442}$ and Trp$^{\alpha 444}$)—are mostly in place in VnfDGK, except for the substitution of Met for His$^{\alpha 451}$ and the substitution of Tyr for Trp$^{\alpha 444}$ (**Figure 7*c***). Finally, the two cofactor ligands in NifDK (Cys$^{\alpha 274}$ and His$^{\alpha 442}$) are conserved in the sequence of VnfDGK, which would allow the cofactor to be secured at its binding site upon insertion (**Figure 7*c***).

BIOSYNTHESIS OF THE P-CLUSTER

In the reduced state, the P-cluster (P^N) of Mo-nitrogenase consists of two [Fe_4S_3] subclusters bridged by a μ_6-sulfur atom (**Figure 1*e***). It is covalently coordinated by six cysteinyl ligands at the α/β-subunit interface of NifDK: three from the α-subunit (Cys$^{\alpha 62}$, Cys$^{\alpha 88}$, and Cys$^{\alpha 154}$) and three from the β-subunit (Cys$^{\beta 70}$, Cys$^{\beta 95}$, and Cys$^{\beta 153}$) (35). Following a two-electron oxidation, however, the P-cluster (P^{OX}) undergoes a change in the core structure, losing two bonds between the Fe atoms of one subcluster and the bridging S and, consequently, rendering this S in a μ_4-coordination (**Figure 1*e***). Accompanying this structural rearrangement, the P^{OX}-cluster gains two more protein ligands: an Oγ ligand from Ser$^{\beta 188}$ and a backbone amide N ligand from Cys$^{\alpha 88}$, which contributes to the overall stability of the relatively open half of the P^{OX}-cluster (**Figure 1*e***) (35). Compared with the P-cluster of the Mo-nitrogenase, the P^V-cluster of the V-nitrogenase assumes a more open conformation and comprises two [Fe_4S_4]-like modules (**Figure 1*g***). Further, the six Cys ligands are conserved in the primary sequence of the α- and β-subunits of VnfDGK (**Figure 7*c***), suggesting that the P^V-cluster is coordinated at the α/β-subunit interface in the same manner as that observed in the case of the P-cluster. Such coordination necessitates an in situ assembly scheme for both P-cluster species (**Figure 2**), which involves the synthesis of these clusters at their respective target locations in NifDK and VnfDGK. As is the case with cofactor assembly, recent biochemical and spectroscopic studies have identified gene products that are essential for a stepwise assembly scheme of the P-cluster (4, 81, 83, 85), coupling two 4Fe units into an 8Fe entity one at a time in the two α/β-subunit halves and working in concert with the insertion of the cofactor to complete the assembly of a functional catalytic component of nitrogenase.

Reductive Coupling of a 4Fe Cluster Pair into an 8Fe P-Cluster

The biosynthesis of the P-cluster, like that of the cofactor, is believed to be launched by NifS and NifU (46–51), which supply [Fe_4S_4] clusters as building blocks for the subsequent assembly of the P-cluster on location at the α/β-subunit interface of NifDK (**Figure 10*a***). The proposal that P-cluster synthesis occurs via the fusion of two 4Fe subclusters was initially based on the geometric symmetry of the P^N-cluster and the observation that attempts to extract the P-cluster from NifDK resulted in the recovery of 4Fe fragments (2). Direct support for this proposal, however, has been obtained only recently through the characterization of two cofactor-deficient forms of NifDK from *A. vinelandii*. One of them (designated Δ*nifB* NifDK) was generated by the deletion of *nifB*, which encodes a protein essential for generating an 8Fe core of the cofactor; the other (designated Δ*nifH* NifDK) was generated by the deletion of *nifH*, which encodes a protein essential for maturing the 8Fe core into a cofactor. The two NifDK variants contain different P-cluster species: Δ*nifB* NifDK carries a normal P-cluster (**Figure 10*b***) (86), which displays a P^{OX}-specific $g = 11.8$ parallel-mode EPR signal in the IDS-oxidized state (**Figure 10*c***)

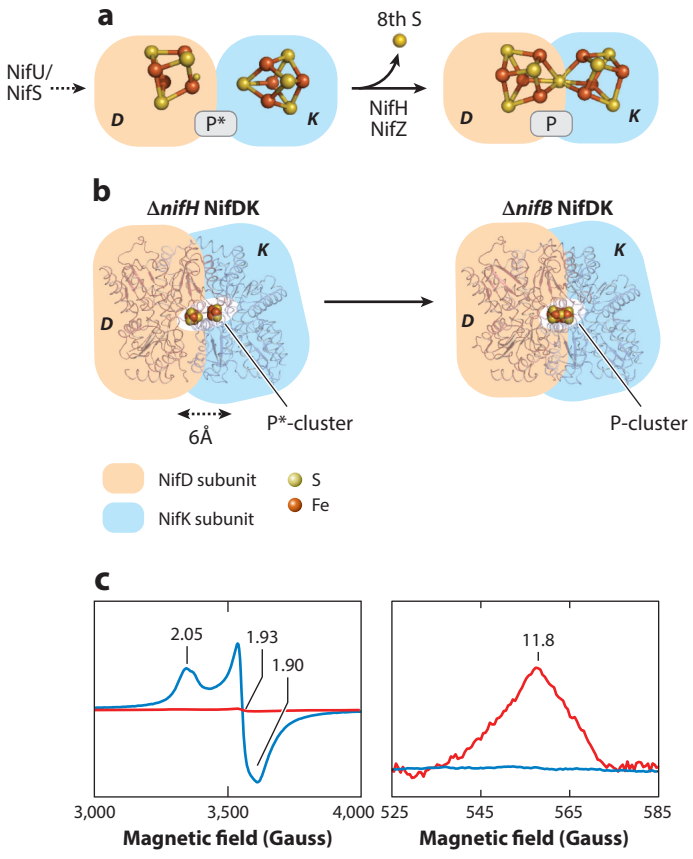

Figure 10

Schematic presentations and spectroscopic analyses of P-cluster formation on NifDK. (*a*) The combined action of NifS and NifU generates $[Fe_4S_4]$-like clusters, which are used to form a P-cluster precursor (designated the P*-cluster). The P*-cluster is comprised of a pair of $[Fe_4S_4]$-like clusters that are located at the α/β-subunit interface of NifDK. The clusters are coupled into a mature $[Fe_8S_7]$ P-cluster concomitant with the removal of one sulfur (S) atom in a process that requires the actions of NifH and NifZ. (*b*) Schematic presentations (highlighted by ribbon diagrams in the background) of (*left*) one αβ-dimer of Δ*nifH* NifDK that contains a P*-cluster and (*right*) one αβ-dimer of Δ*nifB* NifDK that contains a P-cluster. The scheme of Δ*nifH* NifDK was based on small-angle X-ray scattering data and constructed from the structure of holo-NifDK by deletion of the M-cluster, followed by a symmetric 6 Å translation of the D (α)- and K (α)-subunits about the *y* axis. PYMOL (**https://www.pymol.org/**) was used to generate this figure (Protein Data Bank identification numbers: 1M1N and 1L5H). (*c*) Electron paramagnetic resonance spectra of Δ*nifH* NifDK in (*left*) dithionite-reduced and (*right*) indigo disulfonate-oxidized states (*blue*) before and (*red*) after conversion of the P*-cluster to a P-cluster. Upon conversion, (*left*) the P*-specific $S = 1/2$ signal at $g = 2.05$, 1.93, and 1.90 disappears, whereas (*right*) the P^{OX}-specific $g = 11.8$ parallel-mode signal emerges.

(118), whereas Δ*nifH* NifDK carries an unusual P*-cluster, which displays an $[Fe_4S_4]^{1+}$-specific $S = 1/2$ EPR signal in the dithionite-reduced state (**Figure 10*c***) (118). Fe K-edge XAS/EXAFS analyses have revealed that the P*-cluster consists of a typical $[Fe_4S_4]$ cluster and an atypical $[Fe_4S_4]$ cluster (**Figure 10*a***), which either are bridged by a Cys instead of a core sulfide or exist as individual modules, with a light atom (N or O) coordinating the atypical 4Fe module

(119, 120). Magnetic circular dichroism studies have further demonstrated that the P*-cluster was an unbridged 4Fe subcluster pair, comprising one ferredoxin-type $[Fe_4S_4]^{1+}$ cluster and one diamagnetic $[Fe_4S_4]$-like cluster in the dithionite-reduced state (121, 122). The observation of an unbridged pair of $[Fe_4S_4]$-like clusters in Δ*nifH* NifDK is exciting, as this 4Fe cluster pair could very well represent a physiologically relevant intermediate of P-cluster assembly.

Indeed, when Δ*nifH* NifDK was incubated with NifH, MgATP, and dithionite, the P*-cluster-specific $S = 1/2$ EPR signal disappeared in the dithionite-reduced protein, concomitant with the appearance of the P^{OX}-specific $g = 11.8$ EPR signal in the IDS-oxidized protein (**Figure 10*c***) (120). Consistent with the conversion of the P*-cluster to a fully matured P-cluster, Fe K-edge XAS/EXAFS analyses of the Δ*nifH* NifDK protein following such treatment demonstrated a characteristic change of the Fe-Fe backscattering components and an increase in the average Fe-S backscattering distance (120). Accompanying these spectroscopic changes was an increase in the reconstituted activity of this processed NifDK protein, reaffirming the transformation of its P*-cluster into a mature P-cluster (120). Collectively, these results firmly established the P*-cluster as a physiologically relevant precursor to the P-cluster. Interestingly, the maturation of the P-cluster was maximized at certain concentrations of reductant (dithionite) and reductase (NifH), and it had a strict dependence on the hydrolysis of ATP (120). Given that NifH is the only known ATPase in the maturation mixture, this observation suggests that NifH has a critical role in supplying electrons for the reductive coupling of two 4Fe subclusters (P*-cluster) into an 8Fe cluster (P-cluster). Consistent with this suggestion, Fe K-edge XAS analysis has demonstrated a successive reduction of the Fe atoms of the P*-cluster during the maturation process until they eventually stabilize at a near all-ferrous oxidation state (120). Moreover, small-angle X-ray scattering analysis (117) has revealed the presence of a 6 Å gap at the α/β-subunit interface of Δ*nifH* NifDK (containing the P*-cluster) that is absent from the structure of Δ*nifB* NifDK (containing the P-cluster) (**Figure 10*b***), pointing to a role for NifH in bringing the α- and β-subunits of NifDK together while donating electrons to the two $[Fe_4S_4]$ subclusters in the P*-cluster for an efficient coupling of these 4Fe units into an 8Fe P-cluster.

It is not known how the eighth sulfur is eliminated upon the coupling of two $[Fe_4S_4]$ clusters into an $[Fe_8S_7]$ cluster, although certain clues may be provided by the chemical synthesis of analogous model compounds. It has been reported that an $[Fe_8S_7]$ core was chemically synthesized from two all-ferric $[Fe_4S_4]$ clusters via phosphine desulfurization (123). By analogy, one of the $[Fe_4S_4]$ subclusters in the P*-cluster could undergo a similar desulfurization step to eliminate the extra sulfur. It is interesting that, despite the presence of all six P-cluster ligands ($Cys^{\alpha 62}$, $Cys^{\alpha 88}$, $Cys^{\alpha 154}$, $Cys^{\beta 70}$, $Cys^{\beta 95}$, and $Cys^{\beta 153}$) in the sequence of VnfDGK (**Figure 7*c***), the P^V-cluster of V-nitrogenase resembles the P*-cluster much more closely than it does the standard P-cluster, consisting of two relatively separated, $[Fe_4S_4]$-like clusters that display an $[Fe_4S_4]^{1+}$-specific $S = 1/2$ signal in the dithionite-reduced state and no P^{OX}-specific $g = 11.8$ parallel-mode signal in the IDS-oxidized state (41, 43). The presence of an extra, *vnfG*-encoded subunit in VnfDGK may account for the presence of the relatively open structure of the P^V-cluster, as VnfG could interfere with the interaction between VnfH and VnfDGK, and, consequently, impair the VnfH-facilitated reductive coupling of the two 4Fe modules in the P^V-cluster. Moreover, VnfG could provide added stability to the α/β-subunit interface—a feature substituted by the fusion of two 4Fe modules between the α- and β-subunits in NifDK in the absence of such a subunit—thereby eliminating the necessity of fusing the two 4Fe modules into one integral unit in VnfDGK. Nevertheless, the P^V-cluster may still represent an $[Fe_4S_4]$-like cluster pair that is partially processed by VnfH, rendering the two 4Fe modules into a loosely bonded conformation. Clearly, structural information about VnfDGK is needed to conclusively define the conformation of the P^V-cluster and to assess the assembly mechanism of this unique cluster.

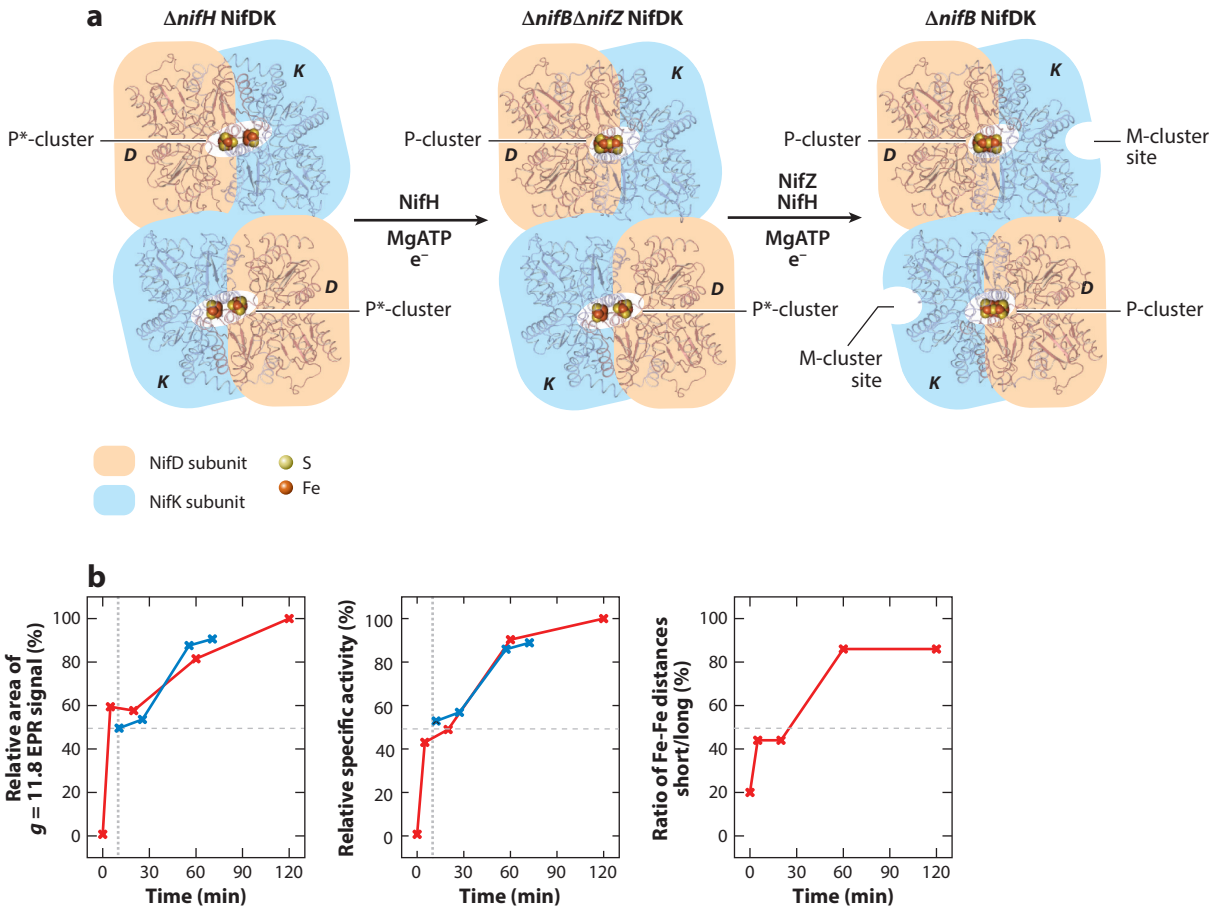

Figure 11

The stepwise assembly of P-clusters on NifDK. (*a*) Different conformations of the P-cluster during the assembly process are represented by (*left*) Δ*nifH* NifDK, which contains two [Fe_4S_4] cluster pairs (or P*-clusters); (*middle*) Δ*nifB*Δ*nifZ* NifDK, which contains one P-cluster and one [Fe_4S_4] cluster pair (or P*-cluster); and (*right*) Δ*nifB* NifDK, which contains two P-clusters. Maturation of the first P-cluster requires NifH, whereas maturation of the second P-cluster requires both NifH and NifZ. The formation of the P-cluster at the α/β-subunit interface also induces a conformational change in the α-subunit, which opens up the M-cluster site. The subunits and atoms are colored as those in **Figure 1**. PYMOL (**https://www.pymol.org/**) was used to generate this figure (Protein Data Bank identification numbers: 1M1N and 1L5H). (*b*) The time-dependent increase in (*left*) the relative area of the P^{OX}-specific $g = 11.8$ parallel-mode electron paramagnetic resonance (EPR) signal, (*middle*) the relative specific activities, and (*right*) the X-ray absorption spectroscopy and extended X-ray absorption fine structure-derived ratio between the short and long Fe-Fe distances of Δ*nifH* NifDK (*red*) and Δ*nifB*Δ*nifZ* NifDK (*blue*). The horizontal dashed lines represent the assembly of the first P-cluster in NifDK, and the vertical dashed lines mark the starting points for the alignment of data acquired for Δ*nifH* NifDK and Δ*nifB*Δ*nifZ* NifDK. Abbreviations: ATP, adenosine triphosphate; Mg, magnesium.

Stepwise Assembly of P-Clusters in Two Subunit Halves

The two P-clusters in NifDK are not synthesized simultaneously; instead, they are assembled one at a time in the two αβ-halves of this protein (**Figure 11*a***). The characterization of a Δ*nifB*Δ*nifZ* NifDK variant of *A. vinelandii*, which was generated by the deletion of *nifB* and *nifZ*, provided the first hint of a stepwise mechanism in P-cluster assembly. In the dithionite-reduced state, Δ*nifB*Δ*nifZ* NifDK displays a P*-cluster-specific $S = 1/2$ signal at approximately 50% of the

intensity displayed by Δ*nifH* NifDK (which contains two P*-clusters); in the IDS-oxidized state, however, it displays the P^{OX}-specific $g = 11.8$ parallel-mode signal at approximately 50% of the intensity displayed by Δ*nifB* NifDK (which contains two P-clusters) (124). Likewise, the magnetic circular dichroism spectrum of Δ*nifB*Δ*nifZ* NifDK overlays almost perfectly with a simulated spectrum comprising the spectra of Δ*nifH* NifDK and Δ*nifB* NifDK at 50% intensity (125). These spectroscopic data also align well with the reconstituted activity of Δ*nifB*Δ*nifZ* NifDK, which is 50% of the reconstituted activity of Δ*nifB* NifDK (124). Together, these observations establish Δ*nifB*Δ*nifZ* NifDK as an intermediary conformation between Δ*nifH* NifDK and Δ*nifB* NifDK, which contains a mature P-cluster in one αβ-half and a P*-cluster (or precursor) in the other αβ-half of NifDK (124, 125). Moreover, NifZ has been identified as an essential factor for the assembly of the second P-cluster in NifDK through these studies. Although the exact function of NifZ is yet to be elucidated, this protein works along with NifH in defining a unique, unsynchronized assembly mechanism for the P-clusters in the two αβ-halves of NifDK.

Interestingly, Δ*nifH* NifDK could be matured stepwise into the conformations of Δ*nifB*Δ*nifZ* NifDK and Δ*nifB* NifDK upon incubation with NifH, MgATP, and dithionite (120). As the incubation time increased, the intensity of the P^{OX}-specific EPR signal increased concomitantly with an increase in the reconstituted activity of this protein, although both had a lag phase at approximately 50% of their respective maximum values (**Figure 11*b***) (120). The 50% P-cluster content achieved during the lag phase represented the formation of one P-cluster in the first αβ-half of the protein, rendering it in the Δ*nifB*Δ*nifZ* NifDK conformation, and the 100% P-cluster achieved at the end of incubation signified the formation of the other P-cluster in the second αβ-half of the protein, rendering it in a Δ*nifB* NifDK conformation (**Figure 11*a***) (120). This assignment was supported further by a good alignment of the spectroscopic changes and activity increases between the post-lag maturation of Δ*nifH* NifDK and the maturation of Δ*nifB*Δ*nifZ* NifDK, which showcased the formation of the P-cluster in the second αβ-half of the protein (**Figure 11*b***) (83, 126). Consistent with these observations, Fe K-edge XAS/EXAFS analysis has supplied further proof of the biphasic maturation of the P-cluster in Δ*nifH* NifDK, demonstrating an unevenly paced shift of Fe K-edge energy throughout the maturation process and a change in the ratio between short and long Fe-Fe distances that occur in two distinct steps (**Figure 11*b***) (120).

P-cluster assembly is coordinated with the insertion of the M-cluster and the overall scheme of NifDK assembly. The maturation of the P-cluster triggers a conformational rearrangement of NifDK, converting the M-cluster site from a closed, inaccessible conformation (represented by Δ*nifH NifDK*) to an open, accessible conformation (represented by Δ*nifB* NifDK) for the subsequent incorporation of the M-cluster (**Figure 11*a***) (86). Consequently, the assembly of the multimeric NifDK occurs in a highly coordinated manner, with the two P-clusters assembled one at a time in the two αβ-halves, followed by the incorporation of the M-cluster upon maturation of the P-cluster in each αβ-half (**Figure 11*a***). Given the homology between the respective α- and β-subunits of NifDK and VnfDGK, a similar coordination can be anticipated for the assembly of VnfDGK. However, the extra (e.g., VnfG) or missing (e.g., "VnfZ") components in the Vnf system will undoubtedly impact and modify the overall assembly scheme of this alternative nitrogenase.

DISCUSSION

Studies of the assembly of nitrogenase metalloclusters have revealed some features shared by the assembly processes of other complex metallocofactors. Most notably, the mobilization of Mo by the ATPase, NifH, could very well exemplify a routine mechanism for metal trafficking in metallocofactor assembly, as the possible formation of a NifH–ADP-Mo intermediate in this process

is paralleled by the appearance of an adenylylated molybdate intermediate in the biosynthesis of molybdopterin cofactors (84), as well as the formation of a similar nucleotide–metal conjugate by CooC (an ATPase analogous to NifH) that facilitates insertion of nickel into the C cluster of carbon monoxide dehydrogenase (CODH) (127). In addition, the insertion of the M-cluster along a pathway into the cluster-binding site of apo-NifDK is mirrored by the insertion of an $[Fe_2S_2]$ cluster along a pathway into the assembly site of apo-HydA1 in the biosynthesis of the H-cluster of the Fe-only hydrogenase, whereas the radical SAM-dependent carbon insertion into the M-cluster is loosely analogous to the radical SAM-dependent attachment of CO, CN^-, and dithiolate ligands to the H-cluster (128–131), both of which highlight certain principles underlying the cluster-transfer and modification steps that occur during the biosynthesis of metallocofactors. Together, these observations establish nitrogenase as an excellent model system for investigating the assembly of complex metallocofactors.

The topological resemblance between the cofactor and P-cluster species of nitrogenase has been illustrated by the successful chemical synthesis of the topologies of both clusters through the rearrangement of similar core structures (132–134). Moreover, such topological similarity underlines the similarity between the biosynthetic routes of the cofactor and P-cluster of nitrogenase. Both pathways follow an iron flow of 1Fe→2Fe→4Fe→8Fe, although the two pathways start to branch beyond the 4Fe stage, which eventually leads to the formation of two structurally and functionally distinct metalloclusters. The biosynthesis of the cofactor involves the coupling of two 4Fe units concomitantly with the insertion of additional elements (i.e., the interstitial carbide and the ninth sulfur) and the rearrangement of the belt sulfur atoms, as well as the replacement of a terminal Fe atom in the 8Fe core by Mo and homocitrate. In comparison, the biosynthesis of the P-cluster involves a simple fusion of the two 4Fe units into an 8Fe core, which also requires the concomitant removal of an eighth sulfur (**Figure 2**). Despite these differences, such variations on the theme of 4Fe fragments implies a coevolution of the cofactor and P-cluster species from 4Fe precursors associated with different protein scaffolds. This theory is supported in part by the observation that BchNB, a NifDK homolog that functions as the catalytic component of dark-operative protochlorophyllide reductase, contains an $[Fe_4S_4]$ cluster at a position analogous to that of the P-cluster in NifDK (135–137). Structural and functional studies of nitrogenase and homologous systems, therefore, will not only provide important insights into the evolution, assembly, and mechanisms of these various metallocenters but also facilitate the future development of strategies to synthesize nitrogenase-based, yet functionally diversified, catalysts for the production of useful products.

DISCLOSURE STATEMENT

The authors are not aware of any affiliations, memberships, funding, or financial holdings that might be perceived as affecting the objectivity of this review.

ACKNOWLEDGMENTS

This work was supported by a grant to M.W.R. from the National Institutes of Health (R01 GM67626).

LITERATURE CITED

1. Burgess BK, Lowe DJ. 1996. Mechanism of molybdenum nitrogenase. *Chem. Rev.* 96:2983–3012
2. Howard JB, Rees DC. 1996. Structural basis of biological nitrogen fixation. *Chem. Rev.* 96:2965–82

3. Eady RR. 1996. Structure–function relationships of alternative nitrogenases. *Chem. Rev.* 96:3013–30
4. Ribbe MW, Hu Y, Hodgson KO, Hedman B. 2014. Biosynthesis of nitrogenase metalloclusters. *Chem. Rev.* 114:4063–80
5. Hoffman BM, Lukoyanov D, Yang ZY, Dean DR, Seefeldt LC. 2014. Mechanism of nitrogen fixation by nitrogenase: the next stage. *Chem. Rev.* 114:4041–62
6. Hu Y, Lee CC, Ribbe MW. 2012. Vanadium nitrogenase: a two-hit wonder? *Dalton Trans.* 41:1118–27
7. Lee CC, Hu Y, Ribbe MW. 2010. Vanadium nitrogenase reduces CO. *Science* 329:642
8. Hu Y, Lee CC, Ribbe MW. 2011. Extending the carbon chain: hydrocarbon formation catalyzed by vanadium/molybdenum nitrogenases. *Science* 333:753–55
9. Lee CC, Hu Y, Ribbe MW. 2011. Tracing the hydrogen source of hydrocarbons formed by vanadium nitrogenase. *Angew. Chem. Int. Ed.* 50:5545–47
10. Rebelein JG, Hu Y, Ribbe MW. 2014. Differential reduction of CO_2 by molybdenum and vanadium nitrogenases. *Angew. Chem. Int. Ed.* 53:11543–46
11. Lee CC, Hu Y, Ribbe MW. 2015. Catalytic reduction of CN^-, CO, and CO_2 by nitrogenase cofactors in lanthanide-driven reactions. *Angew. Chem. Int. Ed.* 54:1219–22
12. Rebelein JG, Hu Y, Ribbe MW. 2015. Widening the product profile of carbon dioxide reduction by vanadium nitrogenase. *ChemBioChem* 16:1993–96
13. Yang ZY, Dean DR, Seefeldt LC. 2011. Molybdenum nitrogenase catalyzes the reduction and coupling of CO to form hydrocarbons. *J. Biol. Chem.* 286:19417–21
14. Yang ZY, Moure VR, Dean DR, Seefeldt LC. 2012. Carbon dioxide reduction to methane and coupling with acetylene to form propylene catalyzed by remodeled nitrogenase. *PNAS* 109:19644–48
15. Schlögl R. 2003. Catalytic synthesis of ammonia—a "never-ending story"? *Angew. Chem. Int. Ed.* 42:2004–8
16. Rofer-DePoorter CK. 1981. A comprehensive mechanism for the Fischer-Tropsch synthesis. *Chem. Rev.* 81:447–74
17. Einsle O, Tezcan FA, Andrade SL, Schmid B, Yoshida M, et al. 2002. Nitrogenase MoFe-protein at 1.16 Å resolution: a central ligand in the FeMo-cofactor. *Science* 297:1696–700
18. Spatzal T, Aksoyoglu M, Zhang L, Andrade SL, Schleicher E, et al. 2011. Evidence for interstitial carbon in nitrogenase FeMo cofactor. *Science* 334:940
19. Kim J, Rees DC. 1992. Crystallographic structure and functional implications of the nitrogenase molybdenum–iron protein from *Azotobacter vinelandii*. *Nature* 360:553–60
20. Lancaster KM, Roemelt M, Ettenhuber P, Hu Y, Ribbe MW, et al. 2011. X-ray emission spectroscopy evidences a central carbon in the nitrogenase iron-molybdenum cofactor. *Science* 334:974–77
21. Tezcan FA, Kaiser JT, Mustafi D, Walton MY, Howard JB, et al. 2005. Nitrogenase complexes: multiple docking sites for a nucleotide switch protein. *Science* 309:1377–80
22. Schindelin H, Kisker C, Schlessman JL, Howard JB, Rees DC. 1997. Structure of ADP•AlF_4^--stabilized nitrogenase complex and its implications for signal transduction. *Nature* 387:370–76
23. Fay AW, Lee CC, Wiig JA, Hu Y, Ribbe MW. 2011. Protocols for cofactor isolation of nitrogenase. *Methods Mol. Biol.* 766:239–48
24. Burgess BK. 1990. The iron-molybdenum cofactor of nitrogenase. *Chem. Rev.* 90:1377–1406
25. Shah VK, Brill WJ. 1977. Isolation of an iron-molybdenum cofactor from nitrogenase. *PNAS* 74:3249–53
26. Lee HI, Hales BJ, Hoffman BM. 1997. Metal-ion valencies of the FeMo cofactor in CO-inhibited and resting state nitrogenase by ^{57}Fe Q-band ENDOR. *J. Am. Chem. Soc.* 119:11395–400
27. Yoo SJ, Angove HC, Papaefthymiou V, Burgess BK, Münck E. 2000. Mössbauer study of the MoFe protein of nitrogenase from *Azotobacter vinelandii* using selective ^{57}Fe enrichment of the M-centers. *J. Am. Chem. Soc.* 122:4926–36
28. Wiig JA, Lee CC, Hu Y, Ribbe MW. 2013. Tracing the interstitial carbide of the nitrogenase cofactor during substrate turnover. *J. Am. Chem. Soc.* 135:4982–83
29. Lee HI, Benton PM, Laryukhin M, Igarashi RY, Dean DR, et al. 2003. The interstitial atom of the nitrogenase FeMo-cofactor: ENDOR and ESEEM show it is not an exchangeable nitrogen. *J. Am. Chem. Soc.* 125:5604–5
30. Moret ME, Peters JC. 2011. N_2 functionalization at iron metallaboratranes. *J. Am. Chem. Soc.* 133:18118–21

31. Pierik AJ, Wassink H, Haaker H, Hagen WR. 1993. Redox properties and EPR spectroscopy of the P clusters of *Azotobacter vinelandii* MoFe protein. *Eur. J. Biochem*. 212:51–61
32. Surerus KK, Hendrich MP, Christie PD, Rottgardt D, Orme-Johnson WH, et al. 1992. Moessbauer and integer-spin EPR of the oxidized P-clusters of nitrogenase: P^{OX} is a non-Kramers system with a nearly degenerate ground doublet. *J. Am. Chem. Soc.* 114:8579–90
33. Watt GD, Burns A, Lough S, Tennent DL. 1980. Redox and spectroscopic properties of oxidized MoFe protein from *Azotobacter vinelandii*. *Biochemistry* 19:4926–32
34. Chan MK, Kim J, Rees DC. 1993. The nitrogenase FeMo-cofactor and P-cluster pair: 2.2 Å resolution structures. *Science* 260:792–94
35. Peters JW, Stowell MH, Soltis SM, Finnegan MG, Johnson MK, et al. 1997. Redox-dependent structural changes in the nitrogenase P-cluster. *Biochemistry* 36:1181–87
36. Joerger RD, Bishop PE. 1988. Bacterial alternative nitrogen fixation systems. *Crit. Rev. Microbiol.* 16:1–14
37. Hales BJ. 1990. Alternative nitrogenase. *Adv. Inorg. Biochem.* 8:165–98
38. Morningstar JE, Johnson MK, Case EE, Hales BJ. 1987. Characterization of the metal clusters in the nitrogenase molybdenum–iron and vanadium–iron proteins of *Azotobacter vinelandii* using magnetic circular dichroism spectroscopy. *Biochemistry* 26:1795–800
39. Harvey I, Arber JM, Eady RR, Smith BE, Garner CD, et al. 1990. Iron K-edge X-ray-absorption spectroscopy of the iron-vanadium cofactor of the vanadium nitrogenase from *Azotobacter chroococcum*. *Biochem. J.* 266:929–31
40. Blank MA, Lee CC, Hu Y, Hodgson KO, Hedman B, et al. 2011. Structural models of the $[Fe_4S_4]$ clusters of homologous nitrogenase Fe proteins. *Inorg. Chem.* 50:7123–28
41. Lee CC, Hu Y, Ribbe MW. 2009. Unique features of the nitrogenase VFe protein from *Azotobacter vinelandii*. *PNAS* 106:9209–14
42. Fay AW, Blank MA, Lee CC, Hu Y, Hodgson KO, et al. 2010. Characterization of isolated nitrogenase FeVco. *J. Am. Chem. Soc.* 132:12612–18
43. Hu Y, Corbett MC, Fay AW, Webber JA, Hedman B, et al. 2005. Nitrogenase reactivity with P-cluster variants. *PNAS* 102:13825–30
44. Dos Santos PC, Dean DR, Hu Y, Ribbe MW. 2004. Formation and insertion of the nitrogenase iron-molybdenum cofactor. *Chem. Rev.* 104:1159–73
45. Kennedy C, Dean D. 1992. The *nifU*, *nifS* and *nifV* gene products are required for activity of all three nitrogenases of *Azotobacter vinelandii*. *Mol. Gen. Genet.* 231:494–98
46. Zheng L, White RH, Cash VL, Dean DR. 1994. Mechanism for the desulfurization of L-cysteine catalyzed by the *nifS* gene product. *Biochemistry* 33:4714–20
47. Zheng L, White RH, Cash VL, Jack RF, Dean DR. 1993. Cysteine desulfurase activity indicates a role for NifS in metallocluster biosynthesis. *PNAS* 90:2754–58
48. Dos Santos PC, Johnson DC, Ragle BE, Unciuleac MC, Dean DR. 2007. Controlled expression of *nif* and *isc* iron–sulfur protein maturation components reveals target specificity and limited functional replacement between the two systems. *J. Bacteriol.* 189:2854–62
49. Smith AD, Jameson GNL, Dos Santos PC, Agar JN, Naik S, et al. 2005. NifS-mediated assembly of [4Fe-4S] clusters in the N- and C-terminal domains of the NifU scaffold protein. *Biochemistry* 44:12955–69
50. Yuvaniyama P, Agar JN, Cash VL, Johnson MK, Dean DR. 2000. NifS-directed assembly of a transient [2Fe-2S] cluster within the NifU protein. *PNAS* 97:599–604
51. Zheng LM, Dean DR. 1994. Catalytic formation of a nitrogenase iron–sulfur cluster. *J. Biol. Chem.* 269:18723–26
52. Christiansen J, Goodwin PJ, Lanzilotta WN, Seefeldt LC, Dean DR. 1998. Catalytic and biophysical properties of a nitrogenase apo-MoFe protein produced by a *nifB*-deletion mutant of *Azotobacter vinelandii*. *Biochemistry* 37:12611–23
53. Paustian TD, Shah VK, Roberts GP. 1990. Apodinitrogenase: purification, association with a 20-kilodalton protein, and activation by the iron-molybdenum cofactor in the absence of dinitrogenase reductase. *Biochemistry* 29:3515–22
54. Hawkes TR, Smith BE. 1983. Purification and characterization of the inactive MoFe protein (NifB-Kp1) of the nitrogenase from *nifB* mutants of *Klebsiella pneumoniae*. *Biochem. J.* 209:43–50

55. Hawkes TR, Smith BE. 1984. The inactive MoFe protein (NifB-Kp1) of the nitrogenase from *nifB* mutants of *Klebsiella pneumoniae*: its interaction with FeMo-cofactor and the properties of the active MoFe protein formed. *Biochem. J.* 223:783–92
56. Shah VK, Allen JR, Spangler NJ, Ludden PW. 1994. In vitro synthesis of the iron-molybdenum cofactor of nitrogenase: purification and characterization of NifB cofactor, the product of NifB protein. *J. Biol. Chem.* 269:1154–58
57. Allen RM, Chatterjee R, Ludden PW, Shah VK. 1995. Incorporation of iron and sulfur from NifB cofactor into the iron-molybdenum cofactor of dinitrogenase. *J. Biol. Chem.* 270:26890–96
58. George SJ, Igarashi RY, Xiao Y, Hernandez JA, Demuez M, et al. 2008. Extended X-ray absorption fine structure and nuclear resonance vibrational spectroscopy reveal that NifB-co, a FeMo-co precursor, comprises a 6Fe core with an interstitial light atom. *J. Am. Chem. Soc.* 130:5673–80
59. Rubio LM, Ludden PW. 2008. Biosynthesis of the iron-molybdenum cofactor of nitrogenase. *Annu. Rev. Microbiol.* 62:93–111
60. Roll JT, Shah VK, Dean DR, Roberts GP. 1995. Characteristics of NifNE in *Azotobacter vinelandii* strains: implications for the synthesis of the iron-molybdenum cofactor of dinitrogenase. *J. Biol. Chem.* 270:4432–37
61. Robinson AC, Burgess BK, Dean DR. 1986. Activity, reconstitution, and accumulation of nitrogenase components in *Azotobacter vinelandii* mutant strains containing defined deletions within the nitrogenase structural gene cluster. *J. Bacteriol.* 166:180–86
62. Filler WA, Kemp RM, Ng JC, Hawkes TR, Dixon RA, et al. 1986. The *nifH* gene product is required for the synthesis or stability of the iron-molybdenum cofactor of nitrogenase from *Klebsiella pneumoniae*. *Eur. J. Biochem.* 160:371–77
63. Robinson AC, Dean DR, Burgess BK. 1987. Iron-molybdenum cofactor biosynthesis in *Azotobacter vinelandii* requires the iron protein of nitrogenase. *J. Biol. Chem.* 262:14327–32
64. Hoover TR, Imperial J, Ludden PW, Shah VK. 1988. Biosynthesis of the iron-molybdenum cofactor of nitrogenase. *BioFactors* 1:199–205
65. Robinson AC, Chun TW, Li JG, Burgess BK. 1989. Iron-molybdenum cofactor insertion into the apo-MoFe protein of nitrogenase involves the iron protein-MgATP complex. *J. Biol. Chem.* 264:10088–95
66. Tal S, Chun TW, Gavini N, Burgess BK. 1991. The Δ*nifB* (or Δ*nifE*) FeMo cofactor-deficient MoFe protein is different from the Δ*nifH* protein. *J. Biol. Chem.* 266:10654–57
67. Gavini N, Burgess BK. 1992. FeMo cofactor synthesis by a *nifH* mutant with altered MgATP reactivity. *J. Biol. Chem.* 267:21179–86
68. Allen RM, Homer MJ, Chatterjee R, Ludden PW, Roberts GP, et al. 1993. Dinitrogenase reductase- and MgATP-dependent maturation of apodinitrogenase from *Azotobacter vinelandii*. *J. Biol. Chem.* 268:23670–74
69. Rangaraj P, Ludden PW. 2002. Accumulation of ^{99}Mo-containing iron-molybdenum cofactor precursors of nitrogenase on NifNE, NifH, and NifX of *Azotobacter vinelandii*. *J. Biol. Chem.* 277:40106–11
70. Zheng LM, White RH, Dean DR. 1997. Purification of the *Azotobacter vinelandii nifV*-encoded homocitrate synthase. *J. Bacteriol.* 179:5963–66
71. Pau RN, Lawson DM. 2002. Transport, homeostasis, regulation, and binding of molybdate and tungstate to proteins. *Met. Ions Biol. Syst.* 39:31–74
72. Hernandez JA, Curatti L, Aznar CP, Perova Z, Britt RD, et al. 2008. Metal trafficking for nitrogen fixation: NifQ donates molybdenum to NifEN/NifH for the biosynthesis of the nitrogenase FeMo-cofactor. *PNAS* 105:11679–84
73. Imperial J, Ugalde RA, Shah VK, Brill WJ. 1984. Role of the *nifQ* gene product in the incorporation of molybdenum into nitrogenase in *Klebsiella pneumoniae*. *J. Bacteriol.* 158:187–94
74. Ugalde RA, Imperial J, Shah VK, Brill WJ. 1985. Biosynthesis of the iron-molybdenum cofactor and the molybdenum cofactor in *Klebsiella pneumoniae*: effect of sulfur source. *J. Bacteriol.* 164:1081–87
75. Rangaraj P, Ruttimann-Johnson C, Shah VK, Ludden PW. 2001. Accumulation of ^{55}Fe-labeled precursors of the iron-molybdenum cofactor of nitrogenase on NifH and NifX of *Azotobacter vinelandii*. *J. Biol. Chem.* 276:15968–74

76. Homer MJ, Dean DR, Roberts GP. 1995. Characterization of the γ protein and its involvement in the metallocluster assembly and maturation of dinitrogenase from *Azotobacter vinelandii*. *J. Biol. Chem.* 270:24745–52
77. Hernandez JA, Igarashi RY, Soboh B, Curatti L, Dean DR, et al. 2007. NifX and NifEN exchange NifB cofactor and the VK-cluster, a newly isolated intermediate of the iron-molybdenum cofactor biosynthetic pathway. *Mol. Microbiol.* 63:177–92
78. Rubio LM, Rangaraj P, Homer MJ, Roberts GP, Ludden PW. 2002. Cloning and mutational analysis of the γ gene from *Azotobacter vinelandii* defines a new family of proteins capable of metallocluster binding and protein stabilization. *J. Biol. Chem.* 277:14299–305
79. Dean DR, Jacobson MR. 1992. Biochemical genetics of nitrogenase. In *Biological Nitrogen Fixation*, ed. G Stacey, RH Burris, HJ Evan, pp. 763–834. New York: Chapman & Hall
80. Hu Y, Ribbe MW. 2013. Biosynthesis of the iron-molybdenum cofactor of nitrogenase. *J. Biol. Chem.* 288:13173–77
81. Hu Y, Ribbe MW. 2013. Nitrogenase assembly. *Biochim. Biophys. Acta* 1827:1112–22
82. Hu Y, Ribbe MW. 2011. Biosynthesis of nitrogenase FeMoco. *Coord. Chem. Rev.* 255:1218–24
83. Hu Y, Ribbe MW. 2011. Biosynthesis of the metalloclusters of molybdenum nitrogenase. *Microbiol. Mol. Biol. Rev.* 75:664–77
84. Schwarz G, Mendel RR, Ribbe MW. 2009. Molybdenum cofactors, enzymes and pathways. *Nature* 460:839–47
85. Hu Y, Fay AW, Lee CC, Yoshizawa J, Ribbe MW. 2008. Assembly of nitrogenase MoFe protein. *Biochemistry* 47:3973–81
86. Schmid B, Ribbe MW, Einsle O, Yoshida M, Thomas LM, et al. 2002. Structure of a cofactor-deficient nitrogenase MoFe protein. *Science* 296:352–56
87. Wiig JA, Hu Y, Ribbe MW. 2011. NifEN-B complex of *Azotobacter vinelandii* is fully functional in nitrogenase FeMo cofactor assembly. *PNAS* 108:8623–27
88. Kaiser JT, Hu Y, Wiig JA, Rees DC, Ribbe MW. 2011. Structure of precursor-bound NifEN: a nitrogenase FeMo cofactor maturase/insertase. *Science* 331:91–94
89. Fay AW, Blank MA, Lee CC, Hu Y, Hodgson KO, et al. 2011. Spectroscopic characterization of the isolated iron-molybdenum cofactor (FeMoco) precursor from the protein NifEN. *Angew. Chem. Int. Ed.* 50:7787–90
90. Corbett MC, Hu Y, Fay AW, Ribbe MW, Hedman B, et al. 2006. Structural insights into a protein-bound iron-molybdenum cofactor precursor. *PNAS* 103:1238–43
91. Lancaster KM, Hu Y, Bergmann U, Ribbe MW, Debeer S. 2013. X-ray spectroscopic observation of an interstitial carbide in NifEN-bound FeMoco precursor. *J. Am. Chem. Soc.* 136:610–12
92. Hutcheson RU, Broderick JB. 2012. Radical SAM enzymes in methylation and methylthiolation. *Metallomics* 4:1149–54
93. Booker SJ. 2012. Radical SAM enzymes and radical enzymology. *Biochim. Biophys. Acta* 1824:1151–53
94. Zhang Q, van der Donk WA, Liu W. 2012. Radical-mediated enzymatic methylation: a tale of two SAMS. *Acc. Chem. Res.* 45:555–64
95. Wiig JA, Hu Y, Lee CC, Ribbe MW. 2012. Radical SAM-dependent carbon insertion into the nitrogenase M-cluster. *Science* 337:1672–75
96. Boal AK, Rosenzweig AC. 2012. Biochemistry: a radical route for nitrogenase carbide insertion. *Science* 337:1617–18
97. Boal AK, Grove TL, McLaughlin MI, Yennawar NH, Booker SJ, et al. 2011. Structural basis for methyl transfer by a radical SAM enzyme. *Science* 332:1089–92
98. Grove TL, Benner JS, Radle MI, Ahlum JH, Landgraf BJ, et al. 2011. A radically different mechanism for *S*-adenosylmethionine-dependent methyltransferases. *Science* 332:604–7
99. Wiig JA, Hu Y, Ribbe MW. 2015. Refining the pathway of carbide insertion into the nitrogenase M-cluster. *Nat. Commun.* 6:8034
100. Frey PA, Hegeman AD, Ruzicka FJ. 2008. The radical SAM superfamily. *Crit. Rev. Biochem. Mol. Biol.* 43:63–88
101. Landgraf BJ, Arcinas AJ, Lee KH, Booker SJ. 2013. Identification of an intermediate methyl carrier in the radical *S*-adenosylmethionine methylthiotransferases RimO and MiaB. *J. Am. Chem. Soc.* 135:15404–16

102. Forouhar F, Arragain S, Atta M, Gambarelli S, Mouesca JM, et al. 2013. Two Fe-S clusters catalyze sulfur insertion by radical-SAM methylthiotransferases. *Nat. Chem. Biol.* 9:333–38
103. Dinis P, Suess DL, Fox SJ, Harmer JE, Driesener RC, et al. 2015. X-ray crystallographic and EPR spectroscopic analysis of HydG, a maturase in [FeFe]-hydrogenase H-cluster assembly. *PNAS* 112:1362–67
104. Knauer SH, Buckel W, Dobbek H. 2011. Structural basis for reductive radical formation and electron recycling in (*R*)-2-hydroxyisocaproyl-CoA dehydratase. *J. Am. Chem. Soc.* 133:4342–47
105. Brigle KE, Weiss MC, Newton WE, Dean DR. 1987. Products of the iron-molybdenum cofactor-specific biosynthetic genes, *nifE* and *nifN*, are structurally homologous to the products of the nitrogenase molybdenum-iron protein genes, *nifD* and *nifK*. *J. Bacteriol.* 169:1547–53
106. Goodwin PJ, Agar JN, Roll JT, Roberts GP, Johnson MK, et al. 1998. The *Azotobacter vinelandii* NifEN complex contains two identical [4Fe-4S] clusters. *Biochemistry* 37:10420–28
107. Hu Y, Fay AW, Ribbe MW. 2005. Identification of a nitrogenase FeMo cofactor precursor on NifEN complex. *PNAS* 102:3236–41
108. Hu Y, Corbett MC, Fay AW, Webber JA, Hodgson KO, et al. 2006. Nitrogenase Fe protein: a molybdate/homocitrate insertase. *PNAS* 103:17125–30
109. Hu Y, Corbett MC, Fay AW, Webber JA, Hodgson KO, et al. 2006. FeMo cofactor maturation on NifEN. *PNAS* 103:17119–24
110. Yoshizawa JM, Blank MA, Fay AW, Lee CC, Wiig JA, et al. 2009. Optimization of FeMoco maturation on NifEN. *J. Am. Chem. Soc.* 131:9321–25
111. Fay AW, Blank MA, Yoshizawa JM, Lee CC, Wiig JA, et al. 2010. Formation of a homocitrate-free iron-molybdenum cluster on NifEN: implications for the role of homocitrate in nitrogenase assembly. *Dalton Trans.* 39:3124–30
112. Georgiadis MM, Komiya H, Chakrabarti P, Woo D, Kornuc JJ, et al. 1992. Crystallographic structure of the nitrogenase iron protein from *Azotobacter vinelandii*. *Science* 257:1653–59
113. Yoshizawa JM, Fay AW, Lee CC, Hu Y, Ribbe MW. 2010. Insertion of heterometals into the NifEN-associated iron-molybdenum cofactor precursor. *J. Biol. Inorg. Chem.* 15:421–28
114. Fay AW, Hu Y, Schmid B, Ribbe MW. 2007. Molecular insights into nitrogenase FeMoco insertion—the role of His 274 and His 451 of MoFe protein α subunit. *J. Inorg. Biochem.* 101:1630–41
115. Hu Y, Fay AW, Ribbe MW. 2007. Molecular insights into nitrogenase FeMo cofactor insertion: the role of His 362 of the MoFe protein α subunit in FeMo cofactor incorporation. *J. Biol. Inorg. Chem.* 12:449–60
116. Hu Y, Fay AW, Schmid B, Makar N, Ribbe MW. 2006. Molecular insights into nitrogenase FeMoco insertion: Trp-$_{444}$ of MoFe protein α-subunit locks FeMoco in its binding site. *J. Biol. Chem.* 281:30534–41
117. Corbett MC, Hu Y, Fay AW, Tsuruta H, Ribbe MW, et al. 2007. Conformational differences between *Azotobacter vinelandii* nitrogenase MoFe proteins as studied by small-angle X-ray scattering. *Biochemistry* 46:8066–74
118. Ribbe MW, Hu Y, Guo M, Schmid B, Burgess BK. 2002. The FeMoco-deficient MoFe protein produced by a *nifH* deletion strain of *Azotobacter vinelandii* shows unusual P-cluster features. *J. Biol. Chem.* 277:23469–76
119. Corbett MC, Hu Y, Naderi F, Ribbe MW, Hedman B, et al. 2004. Comparison of iron-molybdenum cofactor-deficient nitrogenase MoFe proteins by X-ray absorption spectroscopy: implications for P-cluster biosynthesis. *J. Biol. Chem.* 279:28276–82
120. Lee CC, Blank MA, Fay AW, Yoshizawa JM, Hu Y, et al. 2009. Stepwise formation of P-cluster in nitrogenase MoFe protein. *PNAS* 106:18474–78
121. Broach RB, Rupnik K, Hu Y, Fay AW, Cotton M, et al. 2006. Variable-temperature, variable-field magnetic circular dichroism spectroscopic study of the metal clusters in the Δ*nifB* and Δ*nifH* MoFe proteins of nitrogenase from *Azotobacter vinelandii*. *Biochemistry* 45:15039–48
122. Rupnik K, Lee CC, Hu Y, Ribbe MW, Hales BJ. 2011. $[4Fe4S]^{2+}$ clusters exhibit ground-state paramagnetism. *J. Am. Chem. Soc.* 133:6871–73
123. Ohki Y, Tanifuji K, Yamada N, Cramer RE, Tatsumi K. 2012. Formation of a nitrogenase P-cluster $[Fe_8S_7]$ core via reductive fusion of two all-ferric $[Fe_4S_4]$ clusters. *Chem. Asian J.* 7:2222–24

124. Hu Y, Fay AW, Dos Santos PC, Naderi F, Ribbe MW. 2004. Characterization of *Azotobacter vinelandii nifZ* deletion strains: indication of stepwise MoFe protein assembly. *J. Biol. Chem.* 279:54963–71
125. Cotton MS, Rupnik K, Broach RB, Hu Y, Fay AW, et al. 2009. VTVH-MCD study of the Δ*nifB*Δ*nifZ* MoFe protein from *Azotobacter vinelandii*. *J. Am. Chem. Soc.* 131:4558–59
126. Hu Y, Fay AW, Lee CC, Ribbe MW. 2007. P-cluster maturation on nitrogenase MoFe protein. *PNAS* 104:10424–29
127. Jeoung JH, Giese T, Grünwald M, Dobbek H. 2009. CooC1 from *Carboxydothermus hydrogenoformans* is a nickel-binding ATPase. *Biochemistry* 48:11505–13
128. Peters JW, Broderick JB. 2012. Emerging paradigms for complex iron-sulfur cofactor assembly and insertion. *Annu. Rev. Biochem.* 81:429–50
129. Duffus BR, Hamilton TL, Shepard EM, Boyd ES, Peters JW, et al. 2012. Radical AdoMet enzymes in complex metal cluster biosynthesis. *Biochim. Biophys. Acta* 1824:1254–63
130. Berggren G, Adamska A, Lambertz C, Simmons TR, Esselborn J, et al. 2013. Biomimetic assembly and activation of [FeFe]-hydrogenases. *Nature* 499:66–69
131. Esselborn J, Lambertz C, Adamska-Venkatesh A, Simmons T, Berggren G, et al. 2013. Spontaneous activation of [FeFe]-hydrogenases by an inorganic [2Fe] active site mimic. *Nat. Chem. Biol.* 9:607–9
132. Zhang Y, Holm RH. 2004. Structural conversions of molybdenum-iron-sulfur edge-bridged double cubanes and P^N-type clusters topologically related to the nitrogenase P-cluster. *Inorg. Chem.* 43:674–82
133. Zhang Y, Zuo JL, Zhou HC, Holm RH. 2002. Rearrangement of symmetrical dicubane clusters into topological analogues of the P cluster of nitrogenase: nature's choice? *J. Am. Chem. Soc.* 124:14292–93
134. Zhang Y, Holm RH. 2003. Synthesis of a molecular $Mo_2Fe_6S_9$ cluster with the topology of the P^N cluster of nitrogenase by rearrangement of an edge-bridged $Mo_2Fe_6S_8$ double cubane. *J. Am. Chem. Soc.* 125:3910–20
135. Moser J, Langem C, Krausze J, Rebelein J, Schubert WD, et al. 2013. Structure of ADP-aluminium fluoride-stabilized protochlorophyllide oxidoreductase complex. *PNAS* 110:2094–98
136. Bröcker MJ, Schomburg S, Heinz DW, Jahn D, Schubert WD, et al. 2010. Crystal structure of the nitrogenase-like dark operative protochlorophyllide oxidoreductase catalytic complex $(ChlN/ChlB)_2$. *J. Biol. Chem.* 285:27336–45
137. Muraki N, Nomata J, Ebata K, Mizoguchi T, Shiba T, et al. 2010. X-ray crystal structure of the light-independent protochlorophyllide reductase. *Nature* 465:110–14